Polymetallic Complexes for Applications as Photosensitisers in Anticancer Photodynamic Therapy

Patrick S Felder, Sarah Keller, Gilles Gasser

Polymetallic Complexes for Applications as Photosensitizers in Anticancer Photodynamic Therapy

Patrick S. Felder,[a] Sarah Keller,[a] and Gilles Gasser[a,]*

[a] Chimie ParisTech, PSL University, CNRS, Institute of Chemistry for Life and Health Sciences, Laboratory for Inorganic Chemical Biology, F-75005 Paris, France.

* Corresponding author: E-mail: gilles.gasser@chimeparistech.psl.eu; WWW: www.gassergroup.com; Phone: +33 1 44 27 56 02

ORCID Number

Patrick S. Felder: 0000-0003-2325-9026

Sarah Keller: 0000-0003-2667-9157

Gilles Gasser: 0000-0002-4244-5097

Abstract

After the first successful clinical trials of monometallic photosensitizers (PSs) for photodynamic therapy (PDT), the use of polynuclear complexes is currently coming to the fore. These increasingly complex systems bear a high potential to overcome the drawbacks of their mononucleic peers by, for example, increasing the solubility of the PDT PSs and therefore their pharmacokinetic behavior, changing their internal quantum, and singlet oxygen efficiencies or adding supplementary imaging or therapeutical modalities, thus opening up the field for approaches in personalized medicine by combining therapy and diagnosis together in a single treatment. In this review, the most promising examples of polymetallic complexes used as PSs for anticancer PDT are presented.

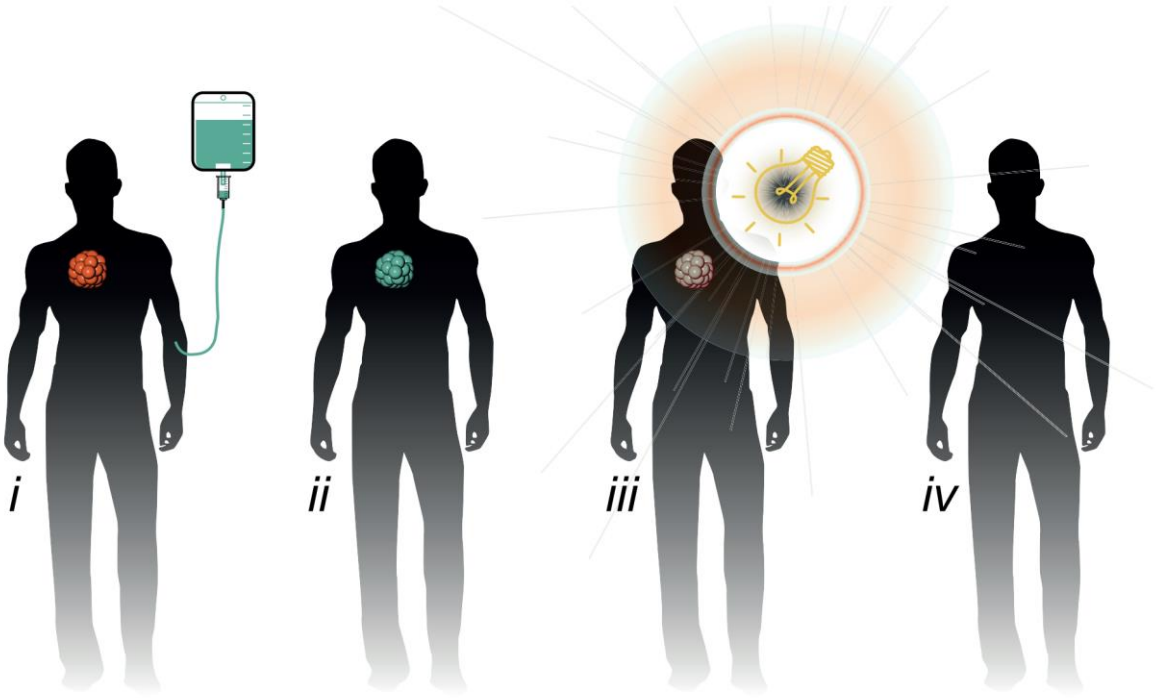

Figure 1. Principle of PDT as a multistep process in cancer therapy: (*i*) Injection of a PS, (*ii*) Accumulation of the PS in the tumor, (*iii*) Local irradiation with (visible) light, (*iv*) Selective treatment of the tumor.

Introduction

Photodynamic therapy (PDT, see Figure 1) has gained significance in medicine over the last twenty years. This rise can in part be attributed to the discovery of several generations of photosensitizers (PSs). The earliest generation is represented by the first clinically established PSs, namely *Photodyn*® (Hematoporphyrin, HpD) and *Photofrin*® (Porfimer Sodium), which are used for ophthalmological and cancer treatments.[1–2] The second generation of PSs, as for example *Foscan*® (Temoporfin) and *Levulan*® (*δ*-Aminolevulinic acid, 5-ALA), were developed to overcome the disadvantages of the first generation such as their low phototoxic index (PI, defined as the ratio between the dark toxicity and phototoxicity) or their slow body excretion rate, which correlates with unspecific cutaneous photosensitivity

for the patients over several days to weeks. Even further down the road, the third generation of PSs were developed to increase the target specificity and their design is based on the combination of a PS with other components such as *in vivo*-activated firefly luciferase, micelles, gap junctional intercellular communication and nanoparticles, assemblies or gels to name some examples.[2]

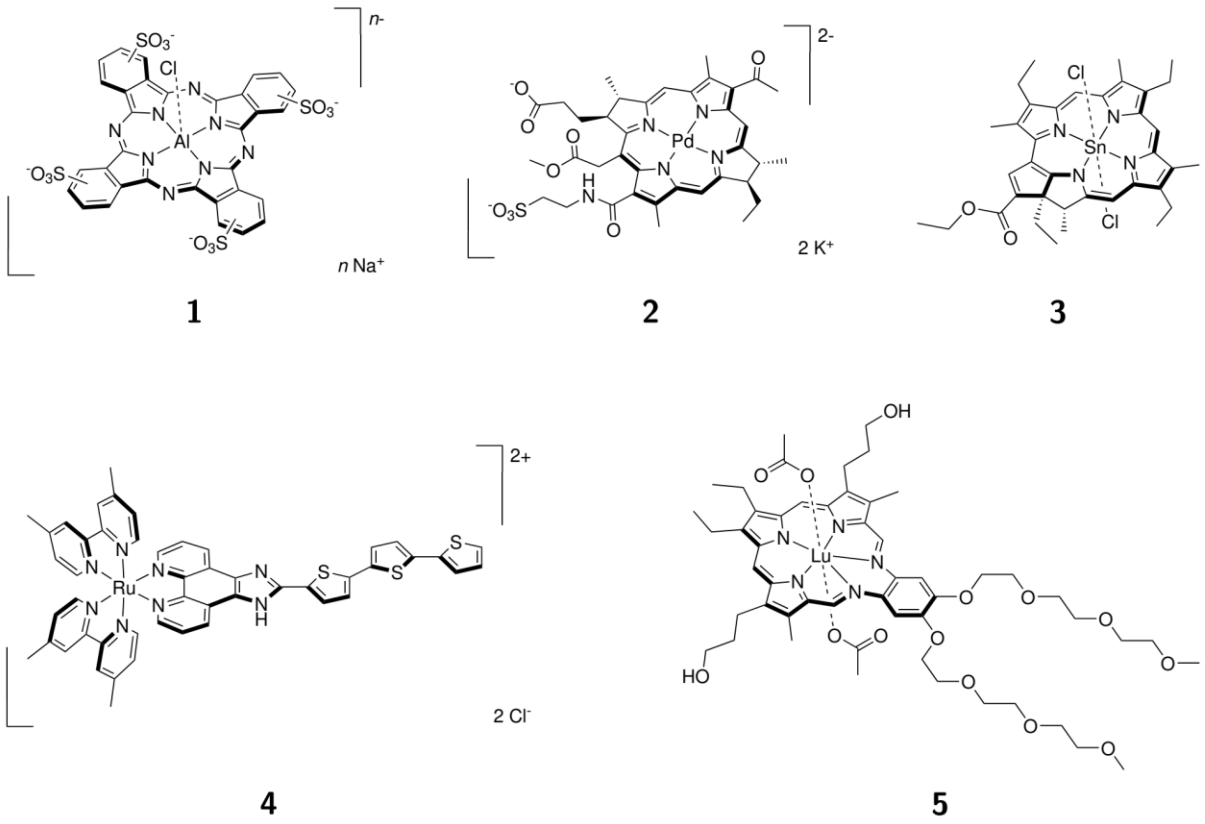

Figure 2. Summary of selected therapeutically important metal-based PDT PSs which have been approved or are currently in clinical trials: $AlPcS_n$ (Photosens, $n = 1$–4, **1**), Padeliporfin (*TOOKAD® soluble*, **2**), SnET2 (Purlytin, **3**), TLD1433 (**4**) and LuTex (Lutrin/Antrin, **5**). [3]

Although metal-free PDT PSs have been dominating the clinical applications so far, metal-containing PSs have finally entered clinical trials, or in several cases already received a local therapeutical approval.[3] To the best of our knowledge, the first metal-based PDT PS which was clinically approved (only in Russia so far) is *Photosens*® (Figure 2: **1**).[4–7] Since November

2017, *TOOKAD® soluble* (**2**, Padeliporfin) was approved in the European Union and in Mexico for the treatment of single-side located low-risk prostate cancer.[8] The phase III study with 413 men with low-risk prostate cancer showed that after 24 months, 49% of the patients treated with **2** had no signs of cancer activity in comparison with 14% of the untreated patients. **2** also showed a delay in the average tumor growth progression of 50% (28 months) in comparison with untreated men (14 months). After successfully passing stage III clinical trials in 2017, **2** entered phase IV which aims to access the undesired post-treatment side effects such as erectile dysfunction, incontinence and related effects which impair the quality of life.[9,10]Three other very promising PDT PS candidates containing metals are in clinical trials, namely Purlytin (Figure 2: **3**), TLD1433 (**4**) and LuTex (**5**, also called Lutrin or Antrin). The tin-based purpurin complex **3** was tested in clinical phase I/II against basal cell carcinomas, metastatic breast cancer and the to the acquired immune deficiency syndrome (AIDS) related Kaposi's sarcoma.[3,11] The ruthenium-based complex **4** developed by McFarland *et al.* is a representative example for the high-potential class of (ruthenium) polypyridyl complexes. **4** has recently successfully passed Phase Ib with six participants for BCG refractory high-risk bon-muscle invasive bladder cancer (NMIBC).[3,12] The fifth candidate **5** is based on a lutetium texaphyrin (Texas-shaped porphyrin) structure which exhibits an outstanding deep tissue-penetration ability e.g. penetration ability as well as an incredibly high accumulation rate in the body which allows for very short therapeutic cycles of just 3 h. The compound is in preclinical studies for recurrent breast cancer and in clinical trials for recurrent prostate and cervical cancer.[11,13] These examples mark the beginning of the era for metal-based PDT PSs and have paved the way for further steps in the drug development processes. The development of a PDT PS is more complex than just optimizing a series of physical, chemical and medicinal parameters to a maximum. An ideal PS is unlikely

to be found. Instead it is more of a screening for a suitable candidate, which can fulfil several aspects of the requested therapeutic effect.[3] Nevertheless, the potential candidates are expected to possess some basic properties. A very relevant attribute which

Table 1. Summary of some therapeutically important values for PDT PSs.[11]

Photosensitizer	*Photofrin*®	*Foscan*®	*TOOKAD*® *soluble* (**2**)	Purlytin (**3**)	Lutrin (**5**)
Absoption [nm]	630	652	763	664	732
Localisation	Golgi Apparatus, plasma membrane	Endoplasmatic reticulum (ER), mitochondria	Vasculature	Mitochondria, Lysosomes	Lysosome
Commonly employed drug-light interval	24–48 h	96 h	15 h	24 h	3 h
Primary mechanism	Vascular damage & ischemic tumor cell necrosis	Vascular damage & direct tumor cytotoxicity	Vascular damage	Direct tumor cytotoxicity	Vascular damage & direct tumor cytotoxicity

has to be considered is the solubility. Many currently established PSs are known for their strong hydrophobicity resulting in an undesired body distribution pattern. This high lipophilicity can lead to a very low body distribution rate, which is visible in the therapeutic intervals (Table 1).[11]

The low body distribution rate is especially a problem for *Photofrin*® with its impressive long plasma half-life time of ≈ 452 h can induce a drug-related photosensitivity for several weeks for the patients.[11] According to the Lipinski's rule of five, the *n*-octanol-water partition coefficient (*log P*) should be below 5.0 (although the exact value is debatable).[14] However, porphyrins easily reach *log P* values of 10.0 or even higher, underlining their poor hydrophilicity.[15] A detailed example on how complexation to a metal can optimize the hydrophilicity and therefore the potential biodistribution, cellular uptake and post-therapeutical excretion of a compound will be described later in detail for perylenequinonoids Hypocrellin A and B.[16–25]

Light penetration in tissue strongly depends on the irradiated wavelength and, of course, the nature of the tissue itself.[1,26] In order to ensure the accessibility of the complete tumor, it is

therefore advantageous if the PSs responds to a wavelength that ensure a maximum penetration depth into the tissue. A comparison between several tissues (Figure 3: human retinoblastoma (black), porcine brain (red), human hand (blue) and melanotic melanoma (green)) revealed that most of them had a window of high penetrability for light between 600 and 900 nm, and the longer the wavelength the deeper the penetration of the light into the tissue. At the bathochromic end, this window is

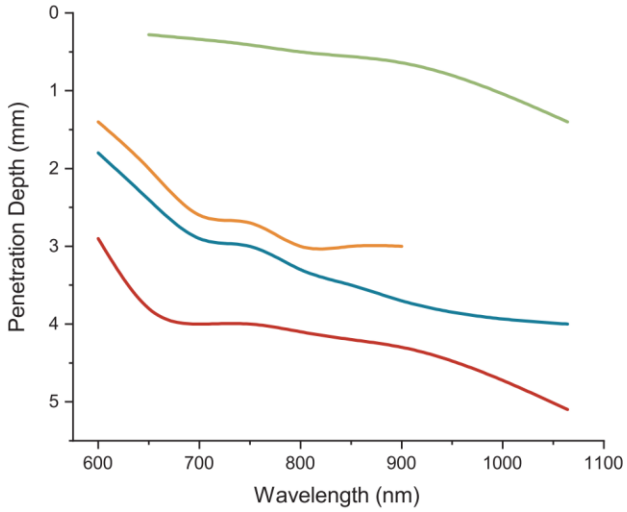

Figure 3. Penetration depth of electromagnetic waves in human retinoblastoma (red), porcine brain (blue), human hand (orange) and melanotic melanoma (green). Graph generated from data from Ogawa et al. [1,26]

predominantly limited by tissue water and fat, whereas undesired absorption at the hypsochromic end is mainly caused by hemoglobin and melanin. Therefore, for many tumor types, it makes sense to aim for compounds with a metal-to-ligand charge transfer (MLCT)-based absorption in the range between 600 and 900 nm, which is known as the phototherapeutic window.[1,26]

Consequently, the photophysical properties of a PDT PS are a key aspect. The absorption of light in the phototherapeutic window between 600 and 900nm is one of the most important parameters. The mechanism of the whole absorption process is explained in detail by the

Jabłonski diagram (Figure 4: top): A PS in the singlet ground state S_0 absorbs (a) a photon and enters a singlet excited state, for example S_1 (PS^*). Besides the internal conversion (ic), the PS^* can leave this excited state again by emission of an energetically lower photon (f = fluorescence) or can, if available, undergo an intersystem crossing (isc) to a triplet excited state T_1 ($^3PS^*$). This triplet state can then be used to create several types of reactive oxygen species (ROS), e.g. superoxide radicals ($O_2^{-\bullet}$) (Figure 4: bottom). In biological systems, $O_2^{-\bullet}$ is quite a dangerous species which can already cause a lot of cellular damage on its own. Therefore, in living organisms, the enzyme superoxide dismutase

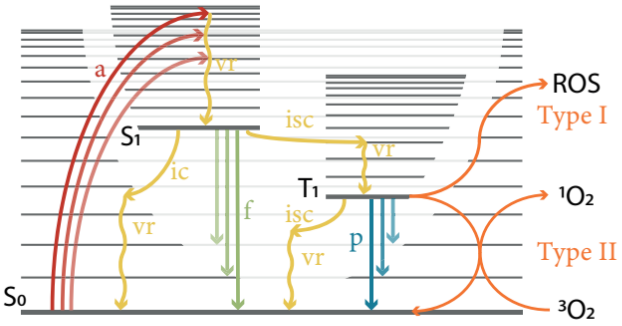

a	= Absorption	isc	= Intersystem crossing
f	= Fluorescence	vr	= Vibrational relaxation
p	= Phosphorescence	ic	= Internal conversion

Type I

$$^3PS^* + {}^3PS^* \longrightarrow PS^{+\bullet} + PS^{-\bullet}$$

$$^3PS^* + \text{Substrate} \longrightarrow \text{Substrate}^{+\bullet} + PS^{-\bullet}$$

$$PS^{-\bullet} + {}^3O_2 \longrightarrow PS + {O_2}^{-\bullet}$$

Type II

$$^3PS^* + {}^3O_2 \longrightarrow PS + {}^1O_2$$

Secondary photochemical reactions

$$2\,{O_2}^{-\bullet} + 2\,H^+ \xrightarrow{\text{SOD}} H_2O_2 + {}^3O_2$$

$${O_2}^{-\bullet} + H_2O_2 \xrightarrow{\text{HaberWeiss}} {}^3O_2 + OH^- + HO^\bullet$$

$${O_2}^{-\bullet} + \text{Fe(III)} \xrightarrow{\text{Fenton}} {}^3O_2 + \text{Fe(II)}$$

$$\text{Fe(II)} + H_2O_2 \xrightarrow{\text{Fenton}} \text{Fe(III)} + OH^- + HO^\bullet$$

Figure 4. Top: Overview showing the different types of radiative and non-radiative transitions in a Jabłoński diagram. Bottom: Mechanistic details of the Type I and Type II processes during photochemical reactions. Both processes can also occur simultaneously. Substrate = biological substrate, SOD = superoxide dismutase.[1,27] Adapted with permission.[1] Copyright 2017, Accounts of Chemical Research.

(SOD) transforms it into hydrogen peroxide (H_2O_2) and molecular triplet oxygen ($^3O_2$).[28] But, since H_2O_2 is highly reactive too, it can undergo a Haber-Weiss or an iron-catalyzed Fenton

reaction to produce hydroxyl radicals (HO•), which are incredibly chemically active and will immediately react with almost any biomaterial in the vicinity.[26] In addition, HO• is also able to induce radical chain cascades, which can cause severe cellular damage at very low concentrations. Depending on the cell phase and cellular localization, this oxidative stress will cause necrosis, paraptosis, apoptosis or other types of cell death.[1] These ROS-induced chain reactions are called Type I mechanism. On the other hand, the $^3PS^*$ can also undergo a Type II mechanism and do a spin exchange with locally present molecular oxygen which is naturally configured in the triplet state ($^3O_2$). As a result, the highly reactive singlet oxygen ($^1O_2$) is produced which is known to cause strong oxidative stress to living cells.[29] $^1O_2$ is metastable and has a relatively long lifetime of $\approx 3\mu s$ in cells, allowing it to spread before it reacts or decomposes.

There are several effects which can induce the probability for an ISC from the S_1 to the T_1 state. ISC is formally forbidden in non-relativistic quantum theory. However, it has been shown that heavy element-related relativistic effects can induce spin-orbit coupling (SOC) and thus lead to highly probable and efficient ISC. Therefore, combining several heavy elements close together in a single complex can have beneficial effects for the quantum yield of every kind of chromophore.[22,30–34]

An important value is the stability of these T_1 states. (Heavy) metals like ruthenium or rhodium can have benefit from their electronic configuration in their excited triplet states (d^5-Ru(II) and d^6-Rh(II)). Excited state lifetimes in the high ns- or low μs-range are not uncommon for ruthenium[35–40] or rhodium[41–49] complexes, which will be discussed in detail later on in this review.

Over the past years, there has been an increasing interest in developing polymetallic complexes as PDT PSs, with various motivations and aims behind this approach. The striking

advantage is that such compounds can comprise two different functionalities. For example, if a (metal-based) PDT PS is combined with cytostatic drugs, a bifunctional molecule is formed which allows for PDT and chemotherapy.[50–54] The aim of this review is to outline the possibilities of polymetallic complexes and their value for the next generation of PDT PSs. Of note, this review is focusing only on compounds with a molecular character as well as metal complexes or metal-containing clusters which were tested as potential candidates for PDT applications. We are mainly focusing on compounds where at least one type of biological experiments was conducted (e.g. DNA cleavage experiments or *in vivo* studies).

Combination of PDT PSs with metal-containing anticancer agents

Since there are already a multitude of established agents for both PDT and cancer related chemotherapy, it is not surprising that scientists have tried to combine some of the most successful examples from both of those therapeutic modalities. It has been shown that the combination of PDT and chemotherapy can significantly increase the success of a cancer treatment.[55] While porphyrins (e.g. *Photofrin*®and *Foscan*®) are regarded as the most established PDT PSs, platinum(II) complexes such as cisplatin, carboplatin and oxaliplatin play the same role in chemotherapy.[2,56] The combination of such systems (Figure 5: **6a–c**) was published by Spingler and coworkers. Their compounds contained 5,10,15,20–tetra(4-pyridyl)porphyrin (TPP) with four tetravalent platinum(II) complexes in three different variations (**6a** = [TPP(Pt(II)–*trans*–$Cl_2DMSO)_4$], **6b** = [TPP(Pt(II)–*cis*–$(NH_3)_2Cl)_4$]), **6c** = [TPP(Pt(II)–*trans*–$(NH_3)_2Cl)_4$].[50] Experiments for the determination of dark and light toxicity in HeLa (human cervical cancer) and CP70 (human ovarian endometrioid adenocarcinoma) cells revealed a significant increase in the PI for the tetra-platinated TPP

complexes **6a–c** (Table 2). Compound **6c** showed an extraordinarily superior PI (1210) in comparison with TPP (PI = 17.3) in HeLa cells.[50] In addition, fluorescence confocal laser scanning microscopy (CLSM, Figure 6) and inductively coupled plasma mass spectrometry (ICP-MS) revealed a complex-induced Pt accumulation in the nucleus of almost 20:1

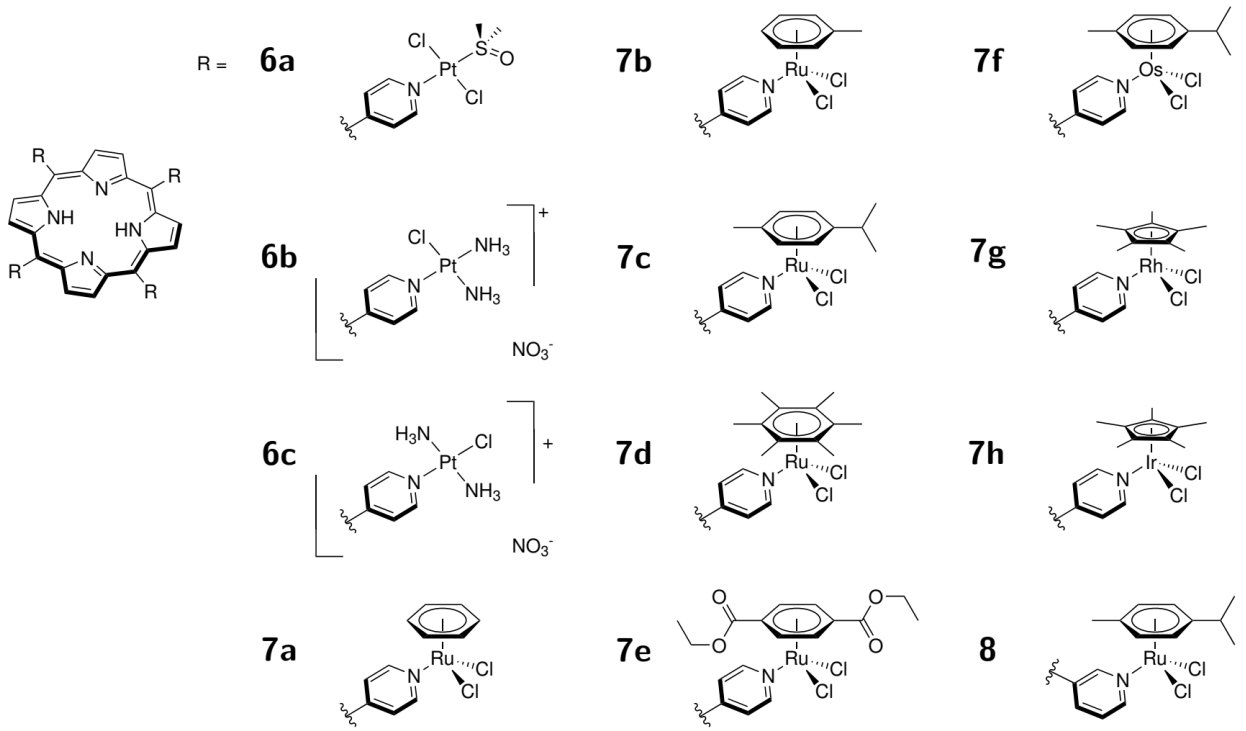

Figure 5. Porphyrin-based PSs coupled to anticancer agents. [50,52]

(versus the cytosol) in HeLa cells. Consequently, the high PI was explained by the strong tendency of TPP to act as a cellular transport shuttle for Pt(II) compounds, which underlined the synergistic properties of the two different therapeutic approaches. Interestingly, the therapeutic efficiency of *trans* complex **6c** was higher than for the corresponding *cis* complex, the opposite of what is observed for cis- and transplatin.[50] Considering the increasing amounts of platinum-resistant tumors, alternatives to the normally omnipotent family of Pt-based anti-cancer drugs are currently

Table 2. Summary of determined PI values for **6a–c** in comparison with the platinum-free TPP and cisplatin.[50]

Compound	PI (HeLA)	PI (CP70)
cisplatin	0.51	0.41
cisplatin + TPP	0.87	–
TPP	17.3	–
6a	>680	1110
6b	655	1930
6c	1210	>5260

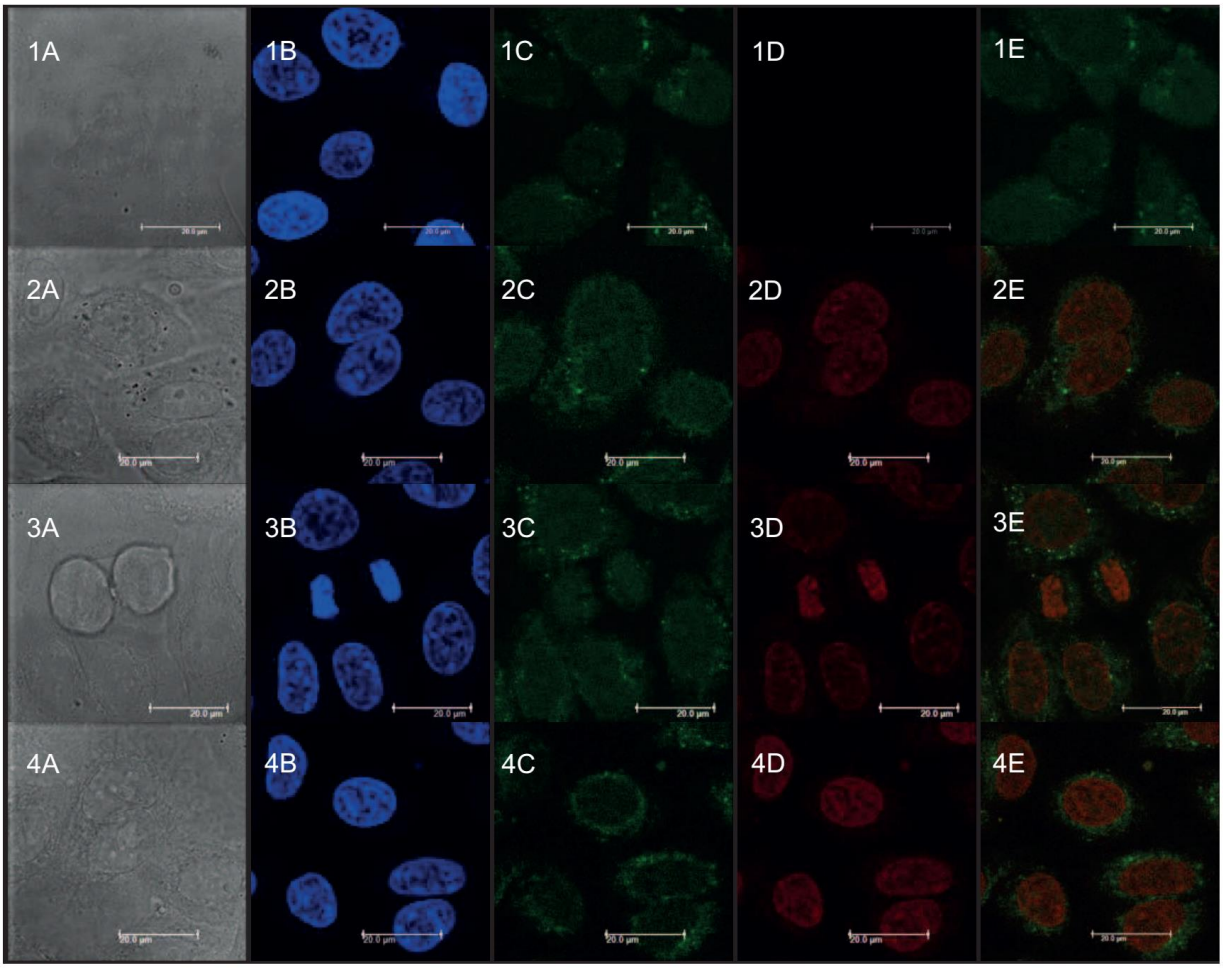

Figure 6. Cellular co-localization of **6a–c** in HeLa cells (1.0 μM). 1: Control; 2-4: **6a–c**; A: Visualized in DIC (differential interference contrast); B: DAPI luminescence images; C: Visualized with MitoTracker Green; D: **6a–c**; E: Merged images A-D (White scale bars: 20 μM). Adapted with permission.[50] Copyright 2014, Wiley-VCH Verlag GmbH & Co. KGaA.

being searched. Ruthenium-based arene and polypyridyl complexes appear to be a promising

class of possible substituents.[57–60] Besides exhibiting activity against Pt-resistant cancer types, many of these ruthenium arene complexes also show anti-metastatic activity and can be selectively transported into cancer cells by transferrin.[52,58,60] An optimized solubility behavior of **7a–e** was

distribution of TPP and platinum, which suggests that the complexes might be stable in cells.[51] already observable during the synthetic procedures since **7a–e** were found to be readily water-soluble.[51] Cellular uptake in Me300 (human melanoma cells) revealed a high uptake for **7a–e** with an accumulation tendency in cytoplasm and certain cell organelles, whereas the rhodium complex **7g** showed no uptake. Investigation of the cellular localization also revealed a similar dark toxity was determined as moderate for **7c**,**d**,**f** (IC_{50} ≈50μm) and low for **7a**,**b**,**e** (IC_{50} >100μm), whereas **7g** showed no cytotoxicity at all. A phototoxicity of 60–80% was achieved for **7a–e** with a dose of 5Jcm^{-2} while for **7f**, a dose of 30Jcm^{-2} was necessary to obtain a similar result.[51] In summary, the authors have found that the differences in absorption, photo- and dark toxicity, cellular uptake and localization between **7a–g** are independent from the arene and just determined by the m *et al.* Consequently, the arene could be of any type of aromatic compound, such as for example targeting agents, inhibitors of resistance mechanisms or other cytotoxic or -static agents.[51] Compound **8** was tested by another group, who found a slightly improved photodynamic efficiency of the 3-pyridiyl derivative in comparison with the 4-pyridiyl compound **7c**.[52] The anti-tumoral activity of **8** was determined during *in vivo* studies with female non-consanguine nude mice (nu/nu). The experiments revealed a mean residence time (MRT) of 85.4h in the plasma, respectively 38.4h in the tumor and a half-life time ($t_{1/2}$) of 58.0h in the plasma and 26.9h in the tumor.[52] ICP-MS experiments confirmed the accumulation of **8** in the liver and the kidneys. The absence of measurable Ru in the brain tissue suggests that **8** seems unable to

cross the blood-brain barrier (BBB).[52] The high (photo)chemical stability, low tendency for photobleaching, low toxicity, as well as their easy tunable solubility behavior make Ru(II) polypyridyl complexes one of the most extensively studied families of PDT PSs.[1,1,3,64–67] As a flagship compound, TLD1433 (see introduction, compound **4**) has just entered phase II clinical trials.[3]

It is therefore not surprising that such an important compound class also contains several polynuclear species. As already shown before, the combination of PDT PSs with platinum-based anti-cancer drugs might have many beneficial effects.[50–52,55] Similar approaches have also been attempted with Ru(II) polypyridyl complexes (Figure 7: **9**).[53] This complex is based on a [Ru(II)dpp_3] center, which is coordinatively saturated by two [Ru(II)bpy_2] systems and cisplatin.[53] Compound **9** binds to DNA (pUC18 plasmids) *via* covalent coordination and light-induced (λ_{Irr} = 450–1000nm) DNA cleavage only take place in the presence of oxygen.[53] Another compound which was successfully tested for DNA binding and cleavage is the bimetallic complex **10**.[61–63] It has been shown that **10** is able to covalently bind to DNA and can induce photocatalytic double-strand cleavage. The absorption in the red-light range due to the 4,7-diphenyl-1,10-phenanthroline (DIP) ligands is especially remarkable. DIP (or bathophenanthroline, Bphen) is already known for its superior DNA-binding capability and is able to induce a bathochromic shift in the emission of

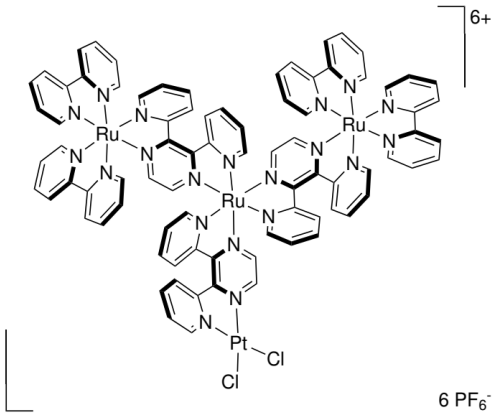

9

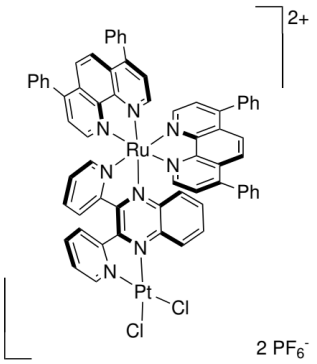

10

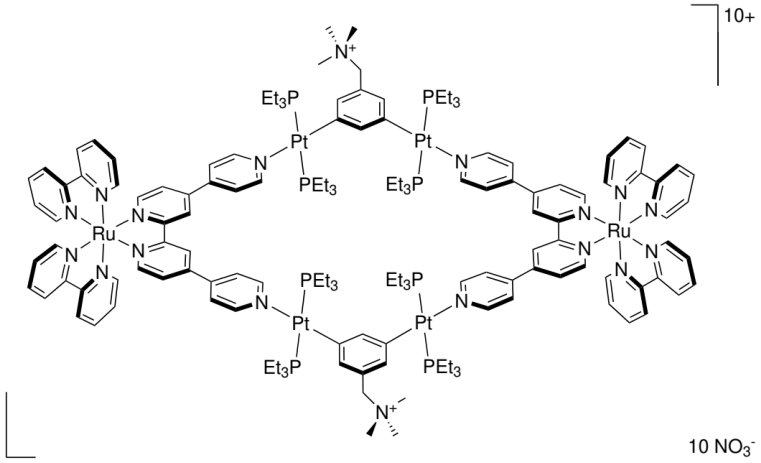

11

Figure 7. Structures of ruthenium-based polynuclear PSs **9**,[53] **10**,[61–63], and **11**[54].

Ru polypyridyl complexes in comparison to other polyazine ligands like bpy or phen.[61–63,68,69] Binding experiments with calf thymus deoxyribonucleic acid (ct-DNA) revealed covalent

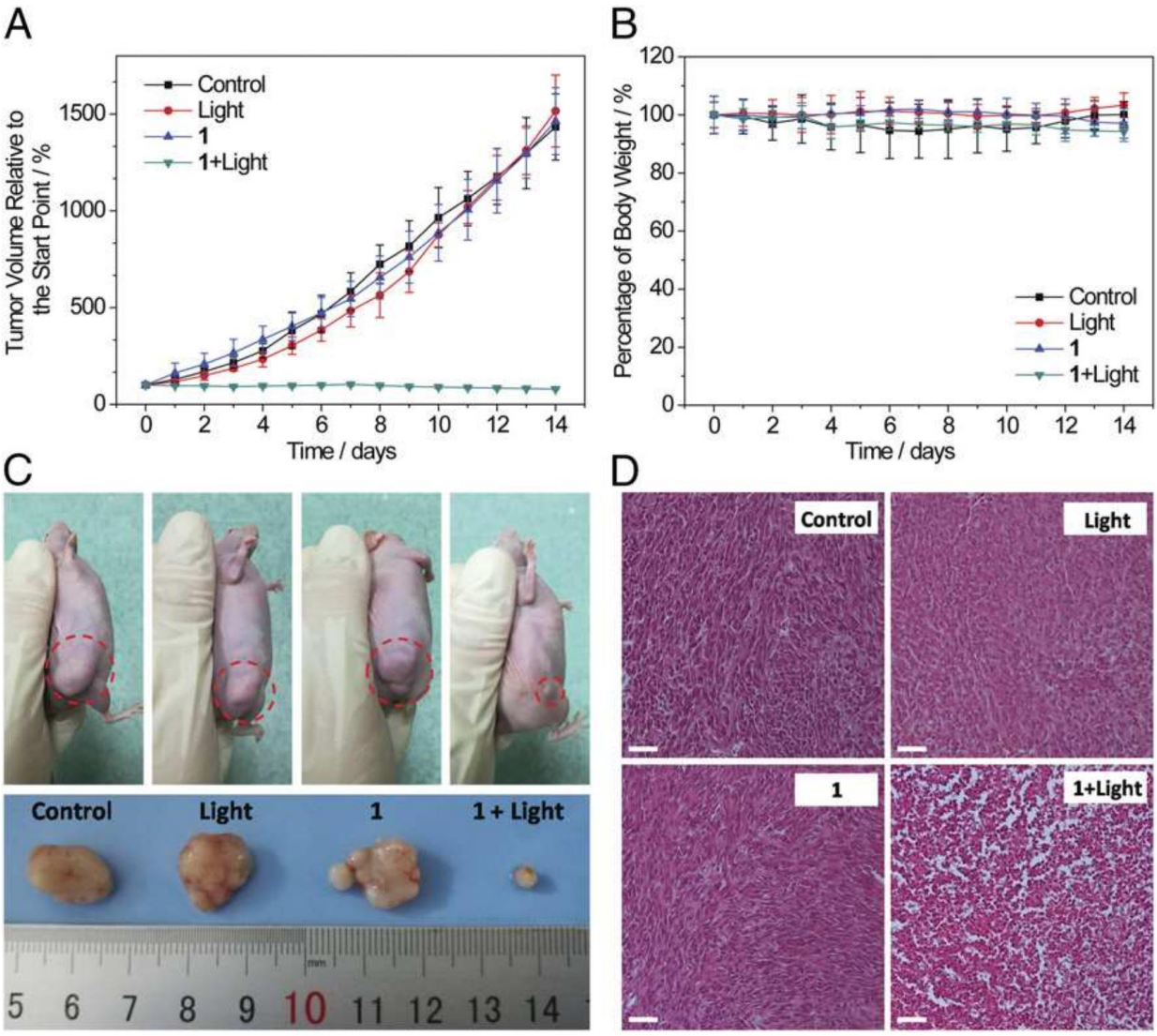

Figure 8. Summary of *in vivo* studies with mice bearing A549 tumors. The mice were divided into four groups: Untreated control, two-photon laser-irradiated control, unirradiated control with direct-injection of **11** (1) into the tumor, two-photon laser-irradiated after direct-injection of **11** (1) into the tumor. A: Growth inhibition curve of the tumors in mice under the four different conditions. A combination of compound **11** (1) under irradiation of light successfully inhibited the tumor growth; B: Average body weight changes of the mice under the four different conditions. The mice showed no significant loss of body weight; C: Representative photographs of the tumors (A549) in mice under the four different conditions; D: Histological examination of the four tumors from figure C (White scale bars: 50 μM). Reproduced with permission.[54] Copyright 2018, National Academy of Sciences of the United States of America.

cisplatin-like binding to DNA with a binding site of ≈32Å.[62] In F98 (rat malignant glioma

cells), complex **10** has shown a low dark toxicity of IC_{50} of >75μm while a light toxicity (T_{Inc} = 48h, λ_{Irr} = 470 nm, 4.35 Jcm^{-2}) IC_{50} of <25μm was achieved.[63]

An example of a two-photon PS is represented by compound **11**[54], which can be synthesized *via* a fast forward auto-assembling reaction of a Ru(II) precursor and a cisplatin derivative. Two-photon PDT has the great advantage that a higher tissue

penetration depth is possible in comparison with the common single-photon PDT. Accumulation of **11** in nuclei and mitochondria of A549 (human pulmonary carcinoma) was confirmed by fluorescence CLSM.[54] PI values were determined in several cancer cell lines (Table 3) and are outstanding in comparison with therapeutically established compounds like 5-ALA. *In vivo* studies in naked mice (Figure 8, n = 14, A549, xenograft tumor volume: 80mm^3) showed a tumor size of 78% in comparison with untreated mice, which exhibited a tumor growth of 1300%.[54]

Overall the combination of a PS like TPP with metal-based (potential) anti-cancer drugs might have some advantages over already therapeutically established drugs. Especially the mono-substituted derivative of **8** showed the potential of polynuclear derivatives over the mono-substituted ones.[52] All discussed compounds **6a–c**, **7a–h**, **8**, **9** and **10** profit from synergistic effects between the organic PS and the coordinated metal complexes.[50–54]

Synergistic Effects of Ruthenium(II)- and Rhodium(II)-based Polynuclear Metal Complexes as PDT PSs

Since the number and the atomic mass of metal centers play a role in the efficiency of a chromophore, a synergistic effect between several metal centers in polynuclear systems can result in better photophysical properties. The achievability of a bathochromic shift towards the desired absorption window, for example, was indirectly demonstrated by Ruminksi *et al.*

by increasing the

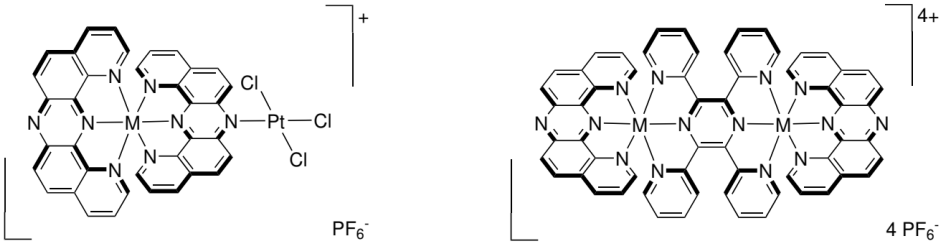

Figure 9. Structures of ruthenium- (and osmium-)based polynuclear PSs **12a**,**b** and **13a**–**c** [33,34]

amount and molecular mass of the coordinated metal centers of compounds **12** and **13** (Figure 9, Table 4).[33,34] Both series of complexes with the ligands dipyrido(2,3-a:3′,2′-j)phenazine (dpop′) and 2,3,5,6-tetra(2-pyridyl)-pyrazine (tppz) showed a significant redshift of the MLCT absorption band due to the influence of the second metal, which underlined the beneficial effect of additional metal centers.[33,34]

A whole series of polynuclear complexes were published by Brewer *et al.*, for example **14**–**18** (Figure 10).[35–40] It was previously shown that $[Rh(III)(phen)_2phi]^{3+}$ and $[Rh(III)(phi)_2bpy]^{3+}$ (phen = 1,10-phenanthroline,phi = 9,10-phen-anthrenequinonediimine, bpy = 2,2′-bipyridine) are able to selectively cleave deoxyribonucleic acid (DNA) *via* C3′-H abstraction under ultraviolet

Table 4. Comparison of the absorption key values for **12a**,**b** and **13a**–**c**.[33,34] The focus is fixed on the PDT relevant parameters: The spectral coverage close to the phototherapeutic window (^{3}MLCT Band), the most bathochromic absorption band (λ_{max}^{ABS}), and the extinsion coefficient ϵ.

Compound		^{3}MLCT Band [nm]	λ_{max}^{ABS} [nm]	ϵ [10^{-4}M^{-1}cm^{-1}]
$[Ru(dpop')_2](PF_6)_2$		$\approx 480-600$	517	2.30
$[Ru(dpop')_2PtCl_3]PF_6$	**12a**	$\approx 500-680$	551	1.64
$[Os(dpop')_2](PF_6)_2$		$\approx 600-780$	713	0.51
$[Os(dpop')_2PtCl_3]PF_6$	**12b**	$\approx 680-850$	751	0.52
$[(dpop')Os(tppz)](PF_6)_2$		$\approx 600-800$	724	0.34
$[(dpop')_2Ru_2(tppz)](PF_6)_4$	**13a**	–	–	–
$[(dpop')_2RuOs(tppz)](PF_6)_4$	**13b**	$\approx 480-850$	700	1.0
$[(dpop')_2Os_2(tppz)](PF_6)_4$	**13c**	$\approx 480-960$	820	0.77

(UV) light in aerobic and anaerobic conditions (see Table 5).[70] Based on these earlier results, Swavey *et al.* published compounds **14a**,**b** (**14a**: M′ = Rh(III), **14b**: M′ = Ir(III))[35–37], **15a**[35] and **16**[35] based on ruthenium(II) and the derivative **14c**[36,37] based on osmium(II) with dpp (2,3bis(2-pyridyl)pyrazine)and bpm (2,2′-bipyrimidine) ligands.[71–73] Complex **14a** showed light-induced DNA cleavage ($\lambda_{Irr} \leq 475$nm) on pUC18 plasmids. Interestingly, this effect was not observable for the iridium-containing derivative **14b** and the bpm-based complex **16**.[35] To further investigate this effect, the ruthenium and bpy in **14a** were replaced by osmium (**14c**), tpy (**15**, tpy = 2,2′:6′,2″-terpyridine) and chloride ligands, respectively.[36] Compounds **14a**,**c** were tested in African green monkey (*Chlorocebus sabaceus*) kidney epithelial (Vero) cell replication assays under exposition of light (Table 5: $\lambda_{Irr} > 460$nm).[37] Since Vero cells are adherent, changes in cell replication rates (after 48h) were detected for the light-exposed cultures and compared with the non-irradiated cells ($cells_{48}h/cells_0 \approx 4.0$). While for **14a** the cell growth factor was reduced to 2.7 (3.0μm), the inhibition effect for **14c** was significantly smaller ($cells_{48}h/cells_0 = 3.4$, c = 5.5$\mu$m).[37] Interestingly, while **14c** reached a maximum inhibition concentration of 110μm with a growth limitation of

Table 5. Summary of the DNA cleavage ability of compounds **14**–**18** for their under light irradiation. [35–40,70]

	Formula	DNA photocleavage?
	$[phen_2Rh(III)phi]$	yes[1]
	$[phi_2Rh(III)bpy]$	yes[1]
	$[bpy_2Ru(II)dpp]$	no
14a	$[(bpy_2Ru(II)dpp)_2Rh(III)]$	yes[2]
14b	$[(bpy_2Ru(II)dpp)_2Ir(III)]$	no
14c	$[(bpy_2Os(II)dpp)_2Rh(III)]$	yes[2]
15	$[(tpyRu(II)dppCl)_2Rh(III)]$	yes[2]
16	$[(bpy_2Ru(II)bpm)_2Rh(III)]$	no
17	$[bpy_2Ru(II)bpmRh(III)phenCl_2]$	yes[2]
18a	$[bpy_2Ru(II)dppRh(III)phenCl_2]$	yes[2]
18b	$[bpy_2Os(II)dppRh(III)phenCl_2]$	yes

[1] Irradiation at $\lambda_{Irr} = 313$ [70]
[2] Irradiation at $\lambda_{Irr} > 460$ [37]

cells$_{48}h$/cells$_0$ = 1.3, **14a** reached an inhibition of cells$_{48}h$/cells$_0$ = 0.13 (c = 120μm) without reaching the maximum inhibition concentration.[37] The different inhibition behavior led to the assumption that compounds **14a**,**c** are using two different mechanisms. In fact, it was just the growth of the cell population that was obstructed, but no significant cytotoxicity was observed with concentrations between 3.0 and 120μm.[37] In the case of bimetallic complexes **17** and **18a**, it was reported that light-induced DNA cleavage occured for both complexes. However, the efficiency of **17** was slightly smaller than for **18a** which was observable in the different irradiation times which were necessary to achive similar results (**18a** t = 10min, **17** t = 60min).[39] It was shown that complex **18b** ($[bpy_2Os(II)dppRh(III)Cl_2phen]^{3+}$) is binding to DNA *via* a light-dependent mechanism and is inhibiting polymerase activity.[38,40] Photobinding and cleavage of DNA were only observed under light irradiation ($\lambda_{Irr} \leq 645$nm) in polymerase chain reaction (PCR) inhibition experiments. Furthermore, **18b** showed a high thermal and (photo)chemical stability since there was no visible decomposition of the compound during the whole PCR procedure (n_{cycles} = 35, T = 94, 58 and 72 °C, t = 180min).[40]

Complexes **19a–c** (Figure) are examples of compounds that Figuwere specifically designed for DNA intercalation.[74] The three dinuclear (bis)bpy_2-complexes are bridged by a 2-imidazolylpyreno[4,5-*d*]imidazole (PyBiimz), which is a strong DNA intercalator (**19a =** $bpy_2Ru(PyBiimz)Rubpy_2$, **19b =** $bpy_2Ru(PyBiimz)Osbpy_2$, **19c =** $bpy_2Os(PyBiimz)Osbpy_2$).[74] The spectroscopically determined data was backed up with *in silico* results.[74] The DNA intercalation constant K_B was determined to be in the order of ≈8.00×10^{5} m^{-1}. Once again, the absorption behavior of the osmium-containing derivatives **19b**,**c** were superior in comparison to the ruthenium complex **19a** (Table 4).[74]

Another example of a DNA-cleaving dinuclear compound is **20**, which was described by Swavey *et al.*[75] Complex **20** showed single and double strand cleavage of circular plasmid DNA (pUC18) under irradiation with a 300W mercury arc lamp. Living tissue was simulated by a low-pass filter cutting wavelengths below 550nm.[75] This complex had a high binding constant K_B of $3.04\pm0.33\times10^{5}$ m^{-1}, which was determined by ct-DNA titration experiments and was explained by DNA intercalation.[75] An interesting compound with great potential is complex **21**.[76] In this new approach, it was attempted to optimize the efficiency of a metal complex by placing a second metal

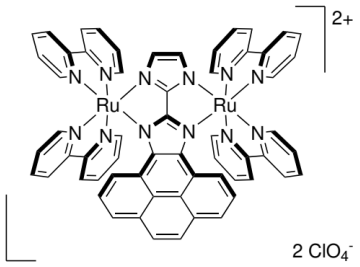

19a : M = 2 Ru^{2+}
19b : M = Ru^{2+}, Os^{2+}
19c : M = 2 Os^{2+}

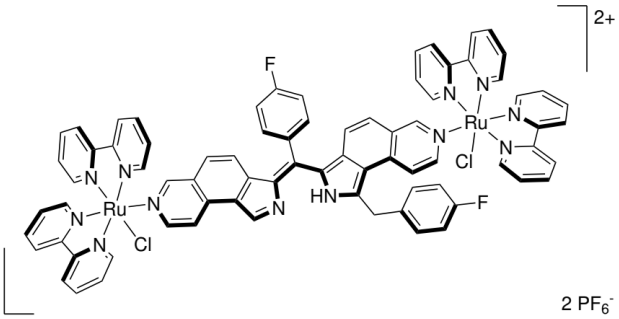

20

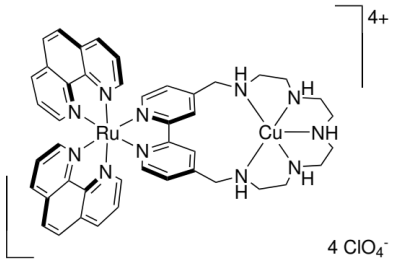

21

Figure 11. Structures of ruthenium- (and osmium-)based dinuclear PSs **19a**,**d** [74], **20** [75] and **21** [76].

close to it. In this case, the copper amine complex plays the role of a redox catalyst. As explained before (see introduction, Figure 4), the Fenton reaction is a key step to increase the ROS cytotoxicity by turning the formed peroxides into hydroxyl radicals (HO•). While iron usually catalyses the classic Fenton reaction, copper and zinc are also able to do so.[27,76] Fluorescence CLSM in A375 (human melanoma cells) indicated that **21** is successfully

internalized into cell compartments such as the nucleus. While the copper-free precursor of **21** showed no cytotoxicity, the IC_{50} value for **21** was quantified to be about 40μl in A375 cells.[76] Interestingly, the amount of light-induced double strand breaks is significantly increased from the copper-free precursor to the final compound **21**, which is a hint for the augmented HO$^{\bullet}$ formation.[76]

The majority of approved PSs work *via* photocatalytic activation of triplet to singlet oxygen. Another option (Figure 12) is provided by photocatalytic enzyme inhibition.[77] Although the concept of selective photoinduced enzyme inhibition is still at an early stage, the approach is quite promising. The principle is based on the photoinduced transformation of a prodrug into an activated metabolite. The complex [Co(III)(acacen)(MeIm)$_2$]Br (**22**, *Doxovir™*, acacen = (4*E*,4′*E*)-4,4′-(1,2-ethanediyldinitrilo)di(2-pentanone), MeIm = 1-Methyl-1*H*-imidazole) was tested for antiviral activity against the drug-resistant *herpes simplex* virus 1.[78] **22** showed an inhibition activity against transport proteins which are necessary for the cellular uptake of the virus.[78] The complex showed no cellular uptake but exhibited a selective irreversible binding and inhibition of transcription factor SP1 *in vitro*. This Zn-finger protein plays a key role in cellular replication and is a potential target for antiviral and antitumoral drug applications.[78]

The activity of **22** and similar Co(III) complexes with labile axial ligands is explained by their binding to the active site of histidine-containing proteins and is demonstrated with the inhibition of enzymes like thermolysin, α-thrombin and MMP-2[79]. Hereby, these Co(III) complexes act as prodrugs and will lose their axial ligands in a biological environment. Interestingly, the combination of **22** or one of its derivatives with a PS such as a Ru(II) polypyridyl complex, the drug activation process can be controlled by light irradiation. Holbrook *et al.* successfully tested a bi-metallic system on the enzyme α-thrombin with an *in*

vitro enzyme assay. A solution of **23a** (100μm), human α-thrombin (4.0unitsml^{-1}) in TRIS (2-amino-2-(hydroxymethyl)propane-1,3diol,

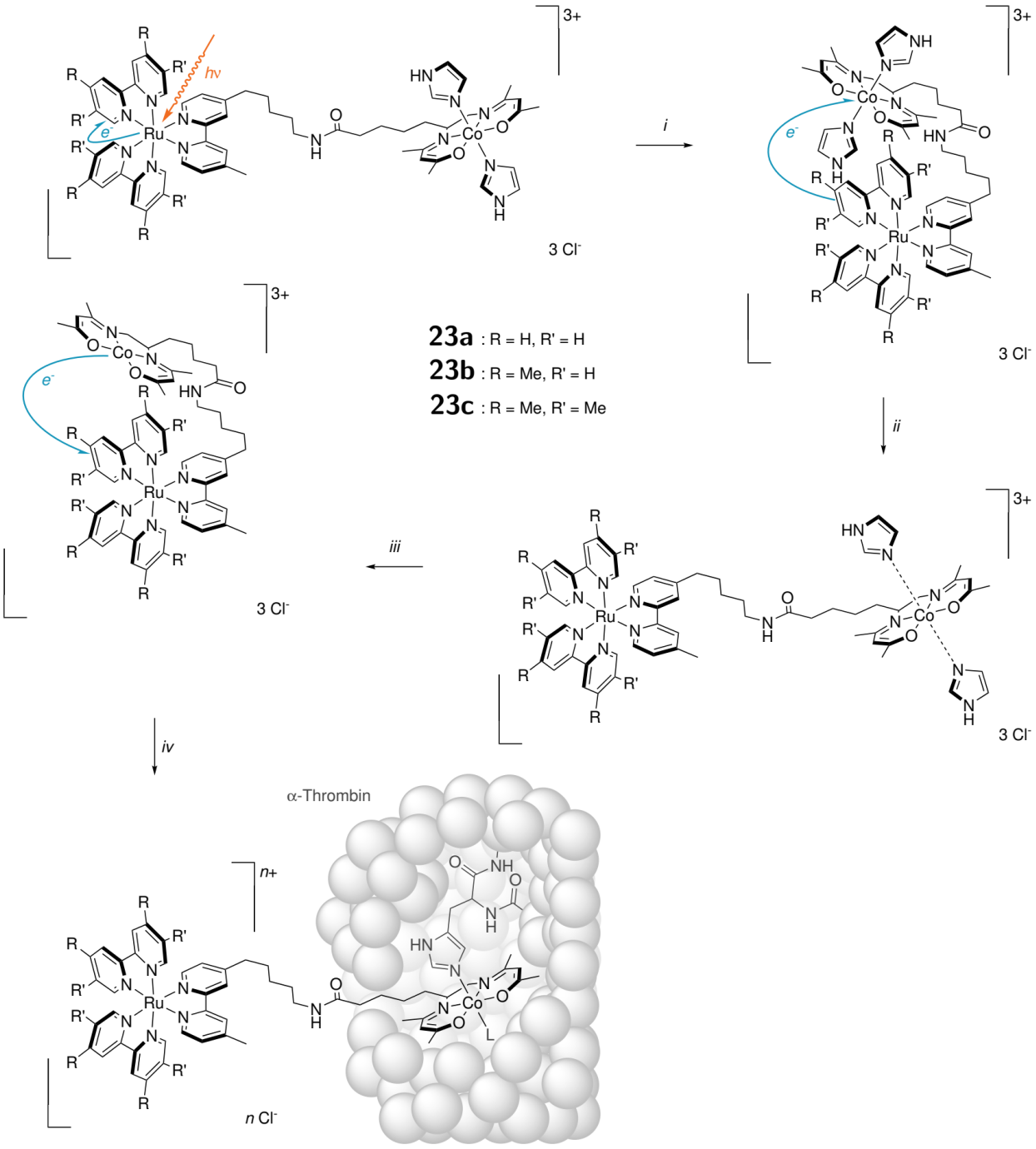

Figure 12. Proposed mechanism of **23a–c** by Holbrook et al. [77]

100mm) and sodium azide (10mm) buffer (pH = 7.4) was diluted over time with more buffer while measuring the enzyme activity of α-thrombin. The serine protease was chosen due to

its key role in the blood coagulation cascade. The authors envisioned that the [Ru(II)bpy$_3$]–[Co(III)acacenL$_2$] conjugate **23a** (L = imidazole) may prevent reocclusion of coronary arteries, which can appear after the thrombolytic therapy of a myocardial infarction.[77] More specifically, under irradiation of light (LED, 4W, $\lambda^{em}{}_{max}$ = 455nm), a significant increase in enzyme activity (k_{dark} = 6.8 × 10^{-5} s^{-1}, *klight* = 3.8 × 10−4 s−1) was observed.[77]

Holbrook *et al.* postulated the following mechanism: In the first step (Figure 12: *i*) the Ru(II)-based PS absorbs a photon and enters an excited state S^1. The electron is transferred from the excited Ru(II)* to the Co(III) complex upon diffusion-controlled physical contact (outer-sphere electron transfer) of the two complexes (*ii*), which is possible due to the flexible link between the two complexes, thus reducing the Co(III) to Co(II). This redox process changes the electron

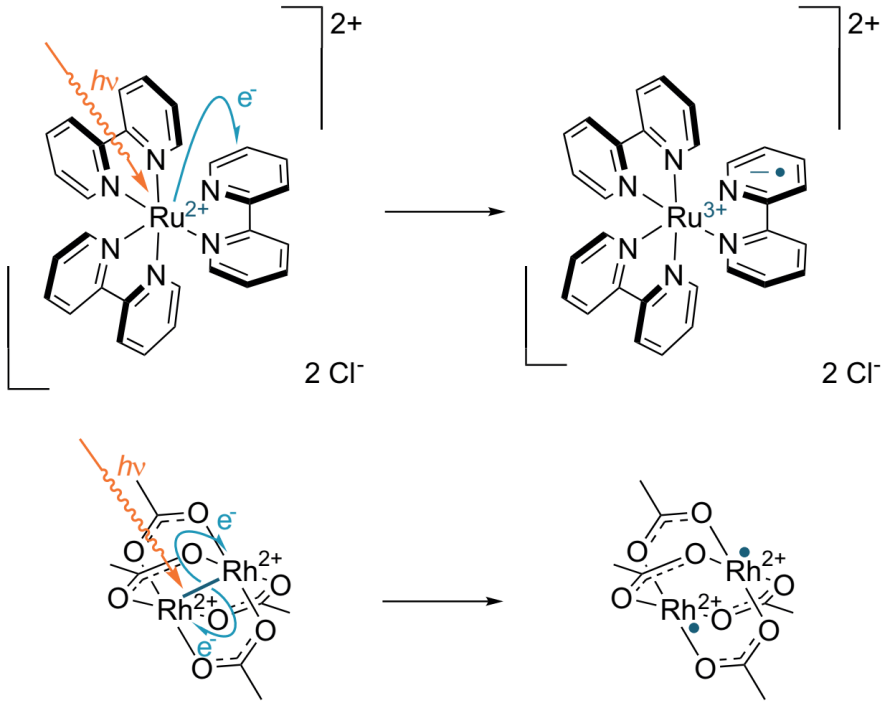

Figure 13. Differences in the activation mechanism: While a mononucleic d^6 complex like $[Ru(bpy)]^{2+}$ is oxidized during charge separation, the binuclear d^7-d^7 complex **24** is forming a diradical. [80,81]

configuration from d^6 to d^7, so that the complex no longer prefers an octahedral geometry

with six ligands. It comes to a loss of the two labile axial imidazole ligands. However, since the Co(II)-d^7 configuration is only metastable in a biological environment, another diffusion-controlled re-oxidation takes place by an electron transfer back to the oxidized Ru(III) complex (*iii*). The square-planar Co(II) species thus formed is now able to occupy the active site of α-thrombin (*iv*) and is sterically protected by the enzyme from re-reduction by another reactivated Ru(II) complex. The α-thrombin is thus irreversibly inhibited.[77]

Similar to the ruthenium polypyridyl complexes, the bi-metallic d^7-d^7 complex dirhodium tetraacetate (Figure 13: **24**) has long-living excited states in the μs-range,

DNA-binding and DNA-polymerase-inhibition properties as well as photoinduced double strand cleavage abilities. All these capabilities are very favorable in view of use as a PDT PS.[41,64] Although many such bi-metallic systems with at least one metal-metal bond are known for their photoactivity (like Mo-Mo, W-W, Pt-Pt and Ir-Ir), none of them are as well studied for photoinduced interaction with DNA as the Rh-Rh complexes. The paddle-wheel shaped di-rhodium complex **24** and its cation $\mathbf{24}^+$ have already shown their large potential for medicinal applications in 1975, when high anti-cancer activities against L1210, Ehrlich ascites, Sarcoma 180 and P388 tumors in mice and tumor cell lines were reported.[64,82] This activity was explained by covalent binding to DNA *via* the axial binding site. After exchange of the coordinated solvent molecules L (Figure 14: **24**), the complexes bind with high affinity to the N, O, P, or S donor atoms. This implies that a coordination to nucleobases (Figure 15) and proteins is possible, which was demonstrated by Chifotides and Dunbar *et al.*[64,82,83] Starting from the basic structure **24**, acetate ligands can be replaced by various bi- and tridentate polypyridyl ligands (**25a**–**e**, **26a**–**e**, **27d**,**e**, **28**, **29** and **30**). The same applies for axial or equatorial ligands, which can be replaced by various solvent molecules.[41–49] In the case of the basic complex **24**, the PS is in need of an electron acceptor such as 3-cyano-1-

methylpyridinium or 1,8-anthraquinone disulfonate. Therefore, the d^7-d^7 dirhodium system is oxidized into a d^6-d^7 complex and *via* photoactivation (λ ≈ 610nm), **24** will induce DNA cleavage trough an anaerobic mechanism.[64,84] Oxygen even seems to have an inhibition function for the activity of **24**.[84] On the other hand, the complex series **26a–d** (Table 6) is induces DNA cleavage *via* a strongly ROS-based mechanism which was not observable for **26e**.[49] The different interactions of **26e** with DNA were explained by an aggregation of the polyanions.[49] It should be mentioned that series **26a–e** is able to cleave DNA under oxygen-free conditions, however with much weaker activity.[49] Consequently, the significant increase of the PI

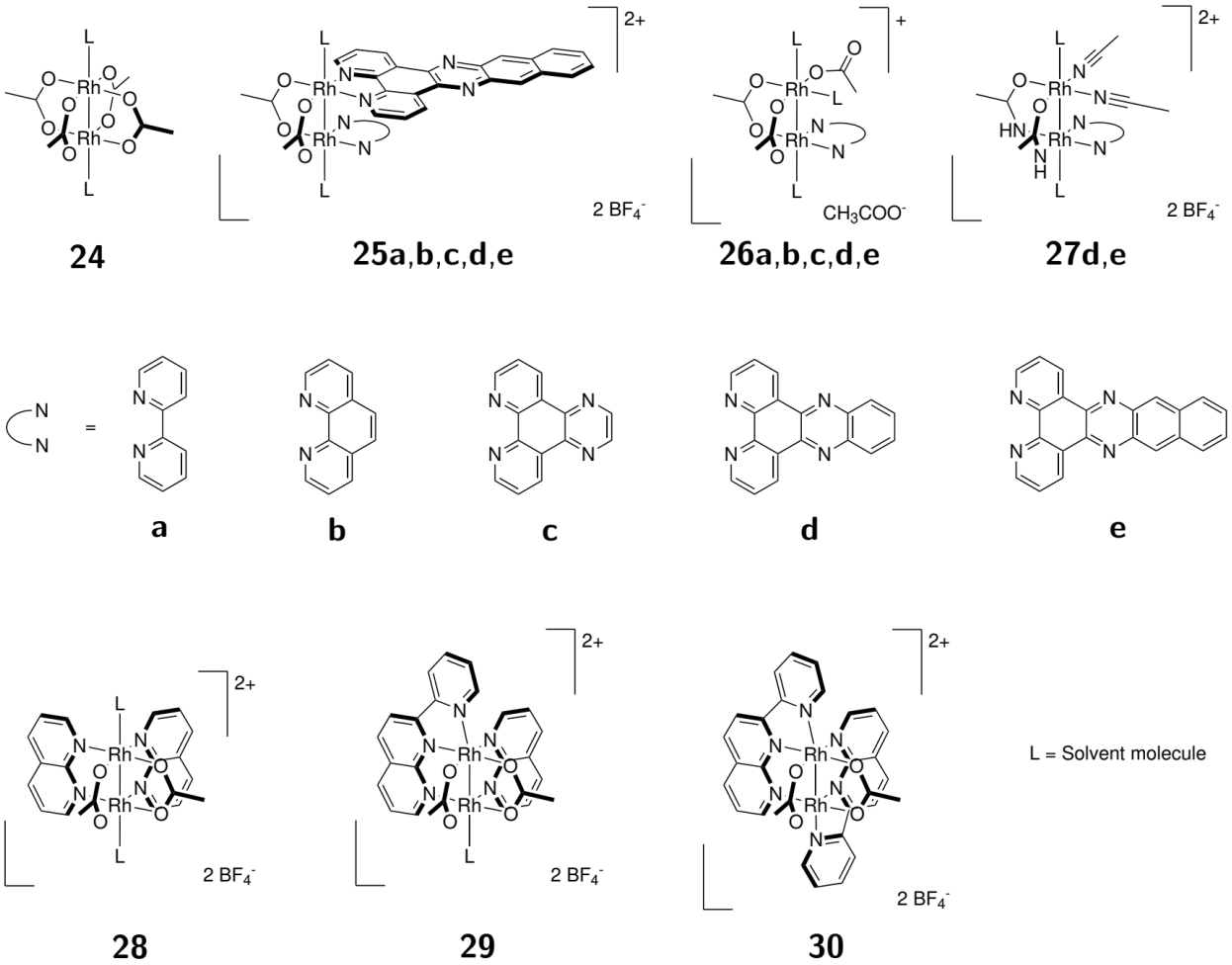

Figure 14. Structures of Rh-Rh compounds developed by Turro et al. [41–49]

Table 6. Photoinduced DNA cleavage of **26a–e** reported by Turro et al. [48,49]

Complex	SSBs [%][1]	LC_{50}^{dark} [μM][2]	LC_{50}^{dark} [μM][3]	LC_{50}^{dark} [μM][4]	LC_{50}^{light} [μM][4,5]	PI[4,5]	$logP$
26a	138 ± 7	92 ± 5	64 ± 3.2	200 ± 20	30 ± 5	6.7	0.32
26b	157 ± 10	87 ± 3	68 ± 3.4	187 ± 17	22 ± 4	8.1	0.30
26c	135 ± 14	91 ± 4	66 ± 3.3	51 ± 5	9 ± 3	5.7	0.41
26d	82 ± 11	68 ± 3.4	68 ± 3	355 ± 18	17 ± 3	21.0	0.62
26e	209 ± 11	201 ± 15	43 ± 2.2	384 ± 24	16 ± 4	24.0	1.02

[1] Single-strand breaks ($SSBs$) in pUC18 plasmid DNA.
[2] In HeLa.
[3] In COLO-316 (ovarian cystadenocarcinoma).
[4] In Hs-27 (human (fore)skin fibroblast).
[5] $\lambda = 400$–700 nm, 30 min.

of **26d**,**e** makes them potential PDT PSs. Besides the DNA cleavage compounds **28**, **29** and **30** also showed a transcription inhibition by stabilizing the duplex DNA *in vitro*.[47]

To summarize this brief overview about the dirhodium complexes, it can be said that they bear a high potential for future application in PDT. The versatility and straightforward tunability of these systems allow for high flexibility, increase of solubility and improved photophysical behavior.

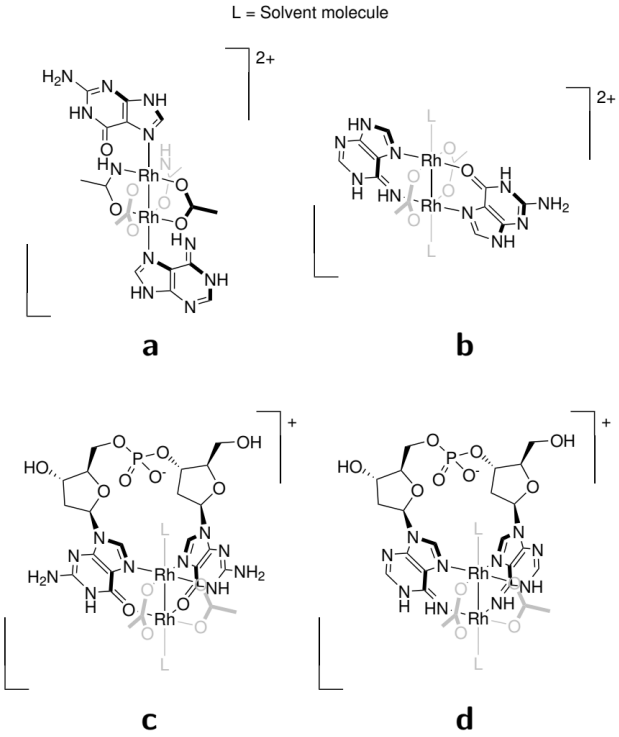

Figure 15. Examples of Rh-Rh complex adducts with the nucleobases guanine (**a**) and adenine (**b**) as well as with the oligonucleotides di-adenosine (**c**) and di-guanosine monophosphate(**d**).

Solubility-tuning by Complexation of Hypocrellin with Transition Metals

The perylenequinonoids Hypocrellin A and B (HA and HB; Figure 16) were found to be molecules of interest in medicinal applications as PDT or anti-HIV agents.[85,86] These naturally occurring PSs which are directly extracted from the bamboo-infesting parasitic fungus *hypocrella bambusae* have a high singlet oxygen quantum yield in benzene (Φ_Δ = 0.84) compared to the values of rose bengal (Φ_Δ = 0.76) or eosin (Φ_Δ = 0.24). HA and HB have a tendency for accumulation in cellular membranes and lysosomes,[86] which makes them potential candidates as a replacement for therapeutically established PDT PSs. Hypocrellins have similar lipophilicity to *Photofrin II*® with significantly faster biodistribution and uptake kinetics.[85] Unfortunately, they are non-light-absorbing in the desired phototherapeutic

window between 600 and 900nm. In order to tackle this drawback, HA and HB were coordinated to (transition) metals.

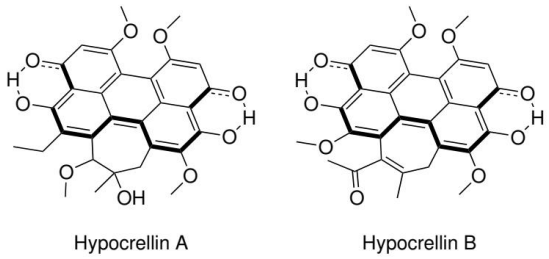

Figure 16. Structures of Hypocrellin A and B.

Hypocrellin-based metal-organic frameworks

The first series of complexes (**32a–n** and **33a–n**; Figure 17) with first row transition metals were described by Diwu and An *et al.*[16,17] They showed high water solubility and the main absorption area could be shifted by almost 200nm towards the deep red range in respect to the free HA and HB molecules, where the first therapeutic window is located. Unfortunately, only the Mg(II)(Φ_Δ = 0.81/0.71) and the Ca(II)HA/HB complexes (Φ_Δ = 0.94/0.79) gave a relative $^1O_2$ production in comparison to the free HA/HB. The absence of $^1O_2$ was explained by an $^1O_2$-inhibition due to the 3*d*-orbitals of the transition metals.[16]. Spectrometric titration of the free HA/HB molecules versus Mg(II) concentration revealed an ideal ligand to metal ratio of 1:1.[16,17] Coordination *via* both phenolate groups was postulated due to the disappearance of the OH-signals in the ^{1}HNMR spectra.[17]

For the first time, experimental investigations about the mechanistic Types I and II were carried out for the corresponding Al(III)-HA-complex (Figure 17: **34**). The presence of the superoxide

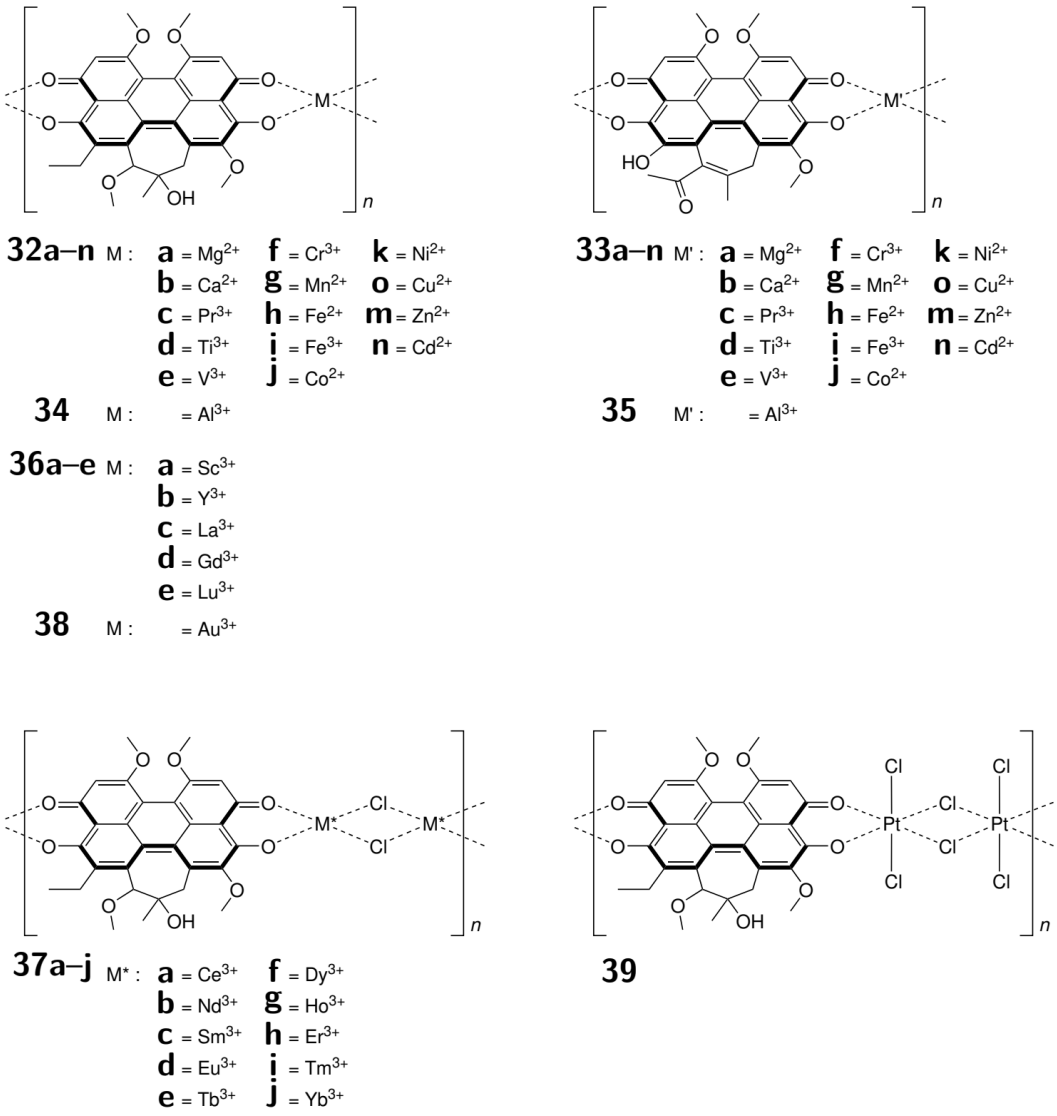

Figure 17. Postulated structures for the HA- and HB complex series **32** and **33** [16,17], **34** [87], **35** [19], **36** and **37** [21], **38** and **39** [22] with the assigned metal ions.

anion $O_2^{\bullet-}$ (Type I) and singlet oxygen $^1O_2$ (Type II) were verified by photoinduced quenching experiments.[87] Hu *et al.* underlined that **34** was more soluble in water than free HA and had a higher chemical stability than the other HA complexes (**32a–n**). The Al(III)-HB complex (**35**; Figure 17) was reported by Ma *et al.*[19] Interestingly, the TypeI activity in the HB complex **35** is twice as high as that of the uncoordinated ligand HB. On the other hand, the free HB showed a three times higher TypeII activity than the corresponding complex **35**. Assumptions about the strutural composition were made based on the characteristic IR

spectra and ^{1}HNMR signals of the quinonoid carbonyl group. Spectrophotometrical titration experiments gave again a consistent result for a metal-organic framework (MOF) like complex formation with a 1:1 HB-Al(III) ratio. Chloride as the corresponding anion was confirmed by precipitation as silver chloride.[19] Due to the enhanced permeability and retention (EPR) effect, a potential higher uptake for several types of cancer cells might be possible for these complexes.[18,20]

The rare earth metal complexes **36** and **37** (Figure 17) with HA were reported by Zeng *et al.*[21] Elemental analysis revealed two different types of complexes. While for Sc(III), Y(III), La(III), Gd(III) and Lu(III) the same composition was obtained as for the first row transition metal ions **32a**–**n** (complexation type X), Ce(III), Nd(III), Sm(III), Eu(III), Tb(III), Dy(III), Ho(III), Er(III), Tm(III) and Yb(III) showed a metal-ligand ratio of 2:1 (**37a**–**j**: complexation type Y). For Pr(III) a ratio of 1.8:1 was unveiled, which did not allow an explicit classification. It turned out that the complexation type (X or Y) had an influence on the luminescence and $^1O_2$ production (Table 7). Only the coordination type X (**36a**–**e**) showed a measurable luminescence and detectable relative $^1O_2$ formation (HAΦ_{Δ}*rel* = 1.0) from 1.32 (La(III)>Gd(III)>Lu(III)>Y(III)>Sc(III) to 0.28. As an exception, only small amounts of $^1O_2$ (0.10), close to the detection limit of the apparatus, could be detected for HA-Tb(III) (**37e**). The complexes **36a**–**e** were also tested for their photodamage ability of ct-DNA (Table 7), which revealed a similar activity pattern as for the $^1O_2$ formation. Therefore,

Table 7. Summary of collected data for **36a–e** and **37a–j**. Reproduced with permission. [21] Copyright 2007, American Chemical Society.

	Formula	e^- conf.	λ_{max}^{abs} [nm][1] λ_{max}^{em} [nm][1]	Φ_F rel.[1]	Φ_Δ rel.[2]	Φ_{ROS} rel.[3]	τ_0 [μs][4] τ_0 [μs][5]	BSR% 10 / 50 [min][6]
	HA		581 / 603	1.00	1.00	1.00	13.0 / 1.68	93.8 / 78.3
36a	HA-Sc^{3+}	$3p^6$	618 / 630	0.48	0.28	0.13	23.0 / 4.04	92.1 / 76.6
36b	HA-Y^{3+}	$4p^6$	620 / 641	0.22	0.50	0.21	112 / 2.53	89.7 / 76.6
36c	HA-La^{3+}	$4f^0$	629 / 637	0.13	1.32	0.29	180 / 1.22	87.1 / 62.4
36d	HA-Gd(III)	$4f^7$	625 / 635	0.11	1.12	0.25	2.60 / 0.55	86.9 / 64.3
36e	HA-Lu^{3+}	$4f^{14}$	623 / 629	0.11	0.75	0.36	88.0 / 2.26	89.3 / 67.2
37a	HA-Ce_2^{3+}	$4f^1$	623 / –	–	<0.05	–	– / –	98.2 / 94.1
37b	HA-Nd_2^{3+}	$4f^3$	619 / –	–	<0.05	–	– / –	98.3 / 93.8
37c	HA-Sm_2^{3+}	$4f^5$	621 / –	–	<0.05	–	– / –	98.4 / 93.4
37d	HA-Eu_2^{3+}	$4f^6$	622 / –	–	<0.05	–	– / –	97.8 / 94.1
37e	HA-Tb_2^{3+}	$4f^8$	626 / 631	0.01	0.10	<0.1	– / –	97.3 / 92.1
37f	HA-Dy_2^{3+}	$4f^9$	628 / –	–	<0.05	–	– / –	97.6 / 93.9
37g	HA-Ho_2^{3+}	$4f^{10}$	623 / –	–	<0.05	–	– / –	98.0 / 92.8
37h	HA-Er_2^{3+}	$4f^{11}$	625 / –	–	<0.05	–	– / –	97.5 / 94.3
37i	HA-Tm_2^{3+}	$4f^{12}$	621 / –	–	<0.05	–	– / –	98.2 / 96.0
37j	HA-Yb_2^{3+}	$4f^{13}$	628 / –	–	<0.05	–	– / –	98.0 / 94.8
	HA-$Pr_{1.8}^{3+}$	$4f^2$	625 / –	–	<0.05	–	– / –	97.7 / 94.8

[1] In DMSO.
[2] In air-saturated DMSO-d_6 determined *via* EPR spin-trapping by use of 2,2,6,6-tetraethyl-4-piperridone (TEMP) after 532 nm laser irradiation.
[3] In argon-saturated DMSO-d_6 determined *via* EPR spin-trapping by use of TEMP after 532 nm laser irradiation.
[4] Time-resolved absorption spectrum technique with 532 nm laser in argon-saturated DMSO.
[5] Time-resolved absorption spectrum technique with 532 nm laser in air-saturated DMSO.
[6] Air-saturated phosphate buffer containing ct-DNA (40 μM) and HA or its metal complex (10 μM), irradiated with > 470 nm by a medium-pressure Na lamp, detecting the remaining binding site (BSR%) of ethidium bromide (80 μM).

the mechanism for photodamaging was assumed to be based on the light-induced $^1O_2$ and $O_2^{\bullet-}$ production. The non-existent phototoxic activity of the **37**-series was explained by the absence of low-energy excited states in the complexes with those metal ions.[21]

Complexes of HA coordinated to Au(III) (**38**) and Pt(IV) (**39**) were published by Zhou *et al.*[22] In comparison to uncoordinated HA, the absorption bands were again red-shifted, closer to the phototherapeutic window. The complexes showed high water solubility ($P_{O/W}$ of HA, **38** and **39**: 9.755, 5.411 and 5.212).[22] Furthermore, the tendency for photobleaching was

significantly lower for **38** (6min at 460nm for HA = 3.80%) and **39** (4.78%) compared to HA (10.16%).[22] Cellular localisation experiments in HeLa cells investigated by CLSM and energy-dispersive X-ray spectroscopy (EDX) demonstrated cytosolic accumulation of HA, **38** and **39**. However, $HAuCl_4$ and H_2PtCl_4 were not taken up by the cells.[22] Irradiation of the treated cells revealed a rather strong light toxicity for HA, **38** and **39** while having a relatively low dark toxicity. Although $HAuCl_4$ was found to produce small amounts of $^1O_2$, almost no phototoxicity was detected (Figure 18). This was explained by the lack of cellular uptake.[22]

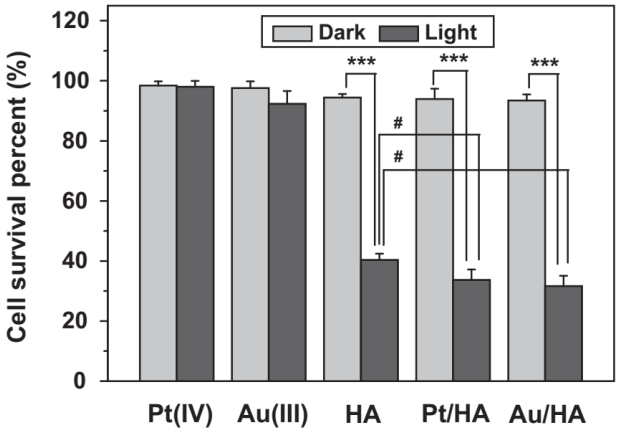

Figure 18. Comparative *in vitro* dark and light toxicity (HeLa cells, ***$p < 0.001$ toxicity of drugs in dark vs : toxicity of drugs after irradiation, #$p < 0.05$ photoinduced toxicity of Pt/HA or Au/HA vs : photoinduced toxicity of HA). Reproduced with permission.[22] Copyright 2013, Elsevier.

Hypocrellin-bridged dinuclear complexes

There are a number of examples where HB acts as a bridging ligand for two polypyridyl complexes, for instance [μ-HB(Ru(II)(bpy)$_2$)$_2$] (Figure 19: **40**), whose redshifted absorption and increased water solubility in comparison to HB are due to the dinuclear coordination.[23] The major advantage of these confined complexes in comparison to the extendend frameworks is that they have a stronger tendency for accumulation in cells. While large metal-organic framework-based complexes **32**-**39** could have potential uptake limitations

due to their high molecular weight, small molecules like **40** might have a better chance for effective cellular uptake. Detailed analysis about

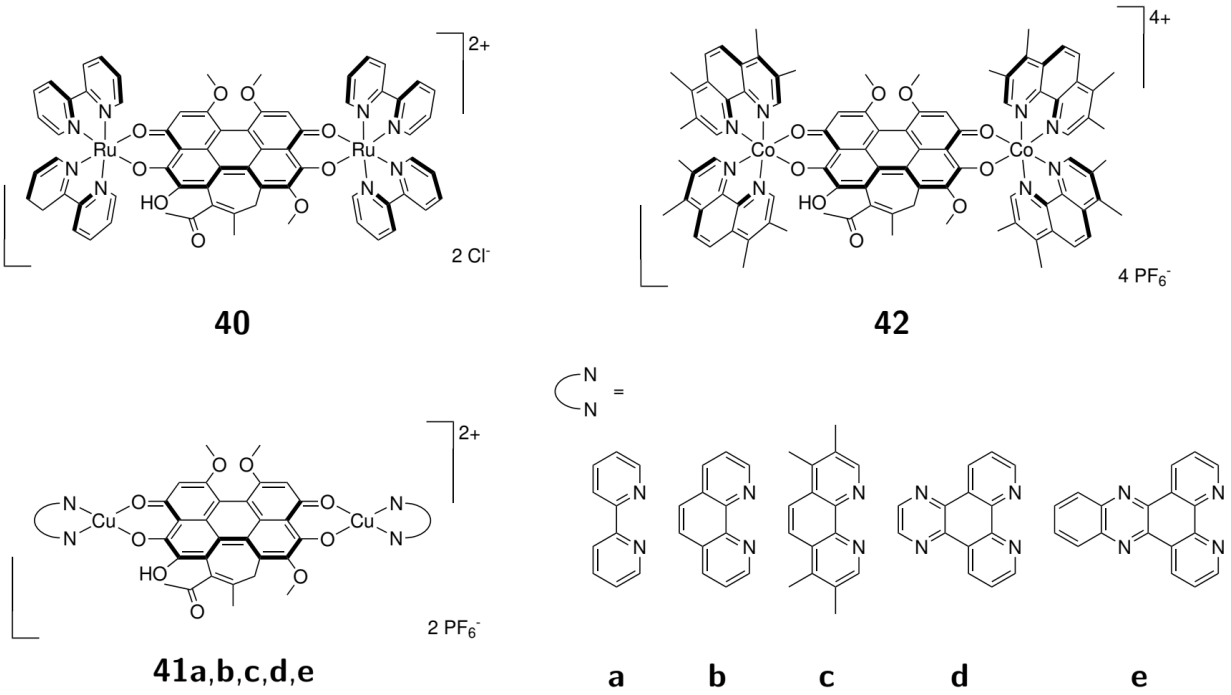

Figure 19. Dinuclear metal complexes of HB with Ru(II) (**40**)[23], Cu(II) (**41a–e**)[24,25] and Co(III) (**42**)[25]

potential application in PDT was performed by Sun *et al.* for [μ-HB(Cu(II)(L))$_2$](PF$_6$)$_2$ (**41a–e**) and [μ-HB(Co(III)(tmp)$_2$)$_2$](PF$_6$)$_4$ (**42**).[24,25] First, the differences in $^1O_2$ production and DNA binding affinity were studied for several bidentate ligands (L) of [μ-HB(Cu(III)(L))$_2$](PF$_6$)$_2$. For this, derivatives with various ligands L **41a** (bpy), **41b** (phen), **41c** (3,4,7,8-tetramethyl-1,10-phenanthroline = tmp), **41d** (dipyrido[3,2f:20,30-h]quinoxaline = dpq) and **41e** (dipyrido[3,2-a:20,30-c]phenazene = dppz)) were synthesised and tested for their photochemically induced nuclease activity. All compounds **41a–e** showed a strong bathochromic shift of about 40nm (the dppz-derivatives of almost 90nm) in comparison to HB, which made them potential candidates for PDT in the first therapeutic window. Compared to HB, the absorbance values of **41a–e** were significantly increased, but

complexes **41a–e** no longer showed any emission. This complete absence of measurable luminescence was explained by the paramagnetic properties of Cu(II). ct-DNA binding experiments revealed different binding constants for the five complexes **41a–e**, with tmp-derivative **41c** giving the highest one. The photoinduced DNA cleavage was identified as mostly $HO^{\bullet}$ and $O_2^{\bullet-}$ driven (TypeI).[24] An even superior DNA binding capability was expected for [μ-HB(Co(III)(tmp)$_2$)$_2$](PF$_6$)$_4$ (**42**) due to its higher charge.[25] However, the expected greater polarity was not observable in DNA binding experiments and *log P* experiments even confirmed a lower polarity for **42** in comparison with **41c**. This was explained by a stronger influence of the two additional lipophilic tmp ligands, which were fully compensating the higher charge of **42**.[25] Surprisingly, while **41c** is mostly $HO^{\bullet}$ and $O_2^{\bullet-}$ driven (TypeI), **42** exhibits a strong $^1O_2$ formation (TypeII).[25]

Combination of PDT and MRI

A crucial step towards personalized medicine is the development of theranostic (i.e. therapy plus diagnosis) treatments, which allow for the diagnosis and the treatment to be done in parallel. This opens up the opportunity to start therapy directly after confirmed successful localization of the drug in the desired tissue.[88]

Magnetic resonance imaging (MRI) is one of the key techniques in localisation and size determination of tumors. To increase the image quality, the use of several gadoliniumbased contrast agents has been common practice for many years. MRI allows visualisation of different tissues depending of their content of hydrogen atoms (mostly bound in water molecules). Due to their paramagnetic character, these Gd(III)-based contrast agents can improve the image quality of T_1 weighed images.[88,90,91] The protons of the exchanging water

molecules that are interacting with the contrast agents have a much shorter relaxation time than the ordinary ones. This difference is observed as a stronger (brighter) signal in the final image. Therefore, modifying the water exchange rate of these Gd(III) complexes and therefore their longitudinal relaxivity r_1 is a key task in the development of MRI contrast agents.[91] In the early studies of the proton relaxation enhancement effect (PRE), it was found that the water exchange rate of several metal complexes bound to a

Table 8. Metal content and relaxivities for the protein-chelated metal ion conjugates. [89]

	# of metal ions[1]	r_1 $[\mathrm{mM}^{-1}\mathrm{s}^{-1}]^2$	r_2 $[\mathrm{mM}^{-1}\mathrm{s}^{-1}]^2$
$[\mathrm{Gd(EDTA)}]^{-1}$	–	3.8	–
$[\mathrm{Gd(DTPA)}]^{-2}$	–	6.6	–
$[\mathrm{Mn(EDTA)}]^{-2}$	–	2.9	–
$[\mathrm{Mn(DTPA)}]^{-3}$	–	1.3	–
IgG–[Gd(EDTA)]	6.3	70	86
IgG–[Gd(DTPA)]	3.6	26	29
IgG–[Mn(EDTA)]	5.3	31	42
IgG–[Mn(DTPA)]	2.5	4.4	4.4
BSA–[Gd(EDTA)]	9.1	66	84
BSA–[Gd(DTPA)]	5.4	19	28
BSA–[Mn(EDTA)]	7.8	32	40
BSA–[Mn(DTPA)]	5.0	3.8	5.1

[1] Per protein molecule.
[2] Per metal ion.

macromolecule was faster than the exchange of the same amount of the analogue free complexes.[92,93] These experiments contained the modification of IgG (bovine immunoglobulin) and BSA (bovine serum albumin) with chelators such as EDTA (2,2′,2″,2‴-(ethane-1,2-diyldinitrilo)tetraacetic acid) and DTPA (2-[bis[2-[bis(carboxymethyl)amino]ethyl]amino]acetic acid). The Gd(III)modified biomolecules indeed showed a considerably higher T_1 relaxivity than would have been obtained by the free complexes with the same Gd(III) concentration in solution (Table 8)[89]. High restrictions

further induce this effect, as for example in large symmetric structures, where the bound Gd complexes have high sterical restrictions in their translational mobility. The combination of a PDT active metal complex with diagnostically suitable metal complexes offers a potential strategy for achieving an efficient theranostic aim.[88] For example, gadolinium compounds typically applied for MRI like *Magnevist*® (Gd-DTPA) or *Dotarem*® (Gd-DOTA = 1,4,7,10-tetraazacyclododecane-*N*,*N*′,*N*″,*N*‴-1,4,7,10-tetra-acetato gadolinium(III)) can be linked with PDT PSs. There were numerous attempts to develop larger, self-organizing and

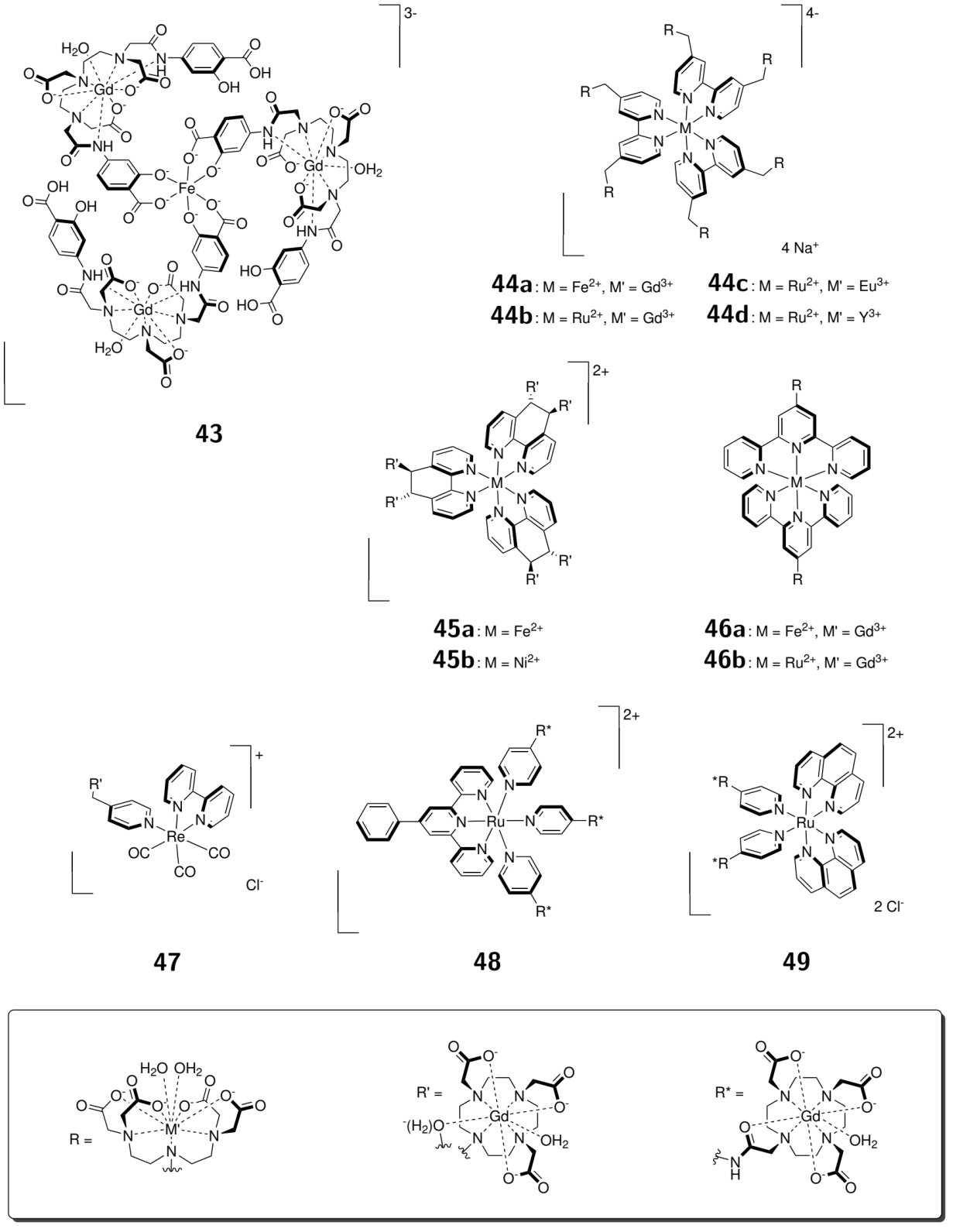

Figure 20. Examples of lanthanide-modified PS for MRI-fluorescence diagnostics. A highly efficient *in situ* formation of the complexes by combining ligands and metal salts in aqueous solution was observable for **43**, **44a**, **45a**,**b** and **46a**. [94–98]

structure-fixing chelators. For example, the octahedral geometry of *in situ*-generated transition metal complexes as a symmetric and structurally well-defined and fixed backbone can fullfill the same task as the proteins IgG and BSA did in earlier attempts. The use of corresponding Fe(II) (Figure 20: **43**, **44a**, **45a** and **46a**)[94–98], Ni(II) (**45b**)[97], Ru(II) (**44b–d**, **46b** and **48**)[98–100] or Re(I) (**47**)[101] polypyridyl complexes (Figure 20) as structural backbones quickly led to the idea to combine highly active MRI contrast agents with optical fluorescence properties. The well analysed "Metallo Star" **44a** has been used several times as an important reference for the PRE effect by researchers investigating new PDT-MRI drug candidates.[95] As a first combination of MRI and PDT agents, a family of Ga-DTPA-modified chlorophyll A compounds (Figure 21: **50a–h**) were developed.[102–104] While complexes **50d–h** were mostly of interest due to their magnetic properties, complexes **50a–c** were directly tested for biological activity in mice (female, C3H/He, implanted RIF tumor). An accumulation of **50a–c** in tumors was observable by MRI scans with injection concentrations between 1.0 and 10.0μm/kg. Due to the low water solubility of **50a**, **50a–c** were administered in a liposomal formulation, which had no influence on the body distribution pattern. In comparison with *Magnevist*®, compound **50c** showed a ten times lower tumor imaging dose (10.0μm/kg, *Magnevist*® = 100.0μm/kg) and reached a maximum tissue concentration after 8h (*Magnevist*® = 10min), which could allow for full body scans due to the longer time window (Figure 22).[102] While **50a**,**b** showed severe side effects like light edema on the tumor imaging dose (10.0μmolkg^{-1}), no light-induced stress reactions were observable for **50c**. Compound **50b** revealed 100% photoinduced lethality on the imaging dose (10.0,μmolkg^{-1}), whereas compound **50c** showed high activity against the RIF tumors after light exposure (130Jcm^{-2} for 30min, 8h postinjection). 80% of the mice were tumor-free after 90 days and showed normal behavior during the whole procedure. Histological analysis

of skin, heart, lungs, liver, kidneys and spleen gave no pathologic evidence of toxicity for **50c** at the tumor imaging dose.[104]

Another approach is based on the idea to combine the therapeutically accepted porphyrin systems with the DTPA-related Gd-DTTA (H_4DTTA = 2,2′,2″,2‴-((azanediylbis(ethane-2,1-diyl))-bis(azanetriyl))tetraacetic acid) complexes (Figure 23). DTTA complexes have the significant advantage of two water molecules coordinated to the Gd(III) center (instead of just one

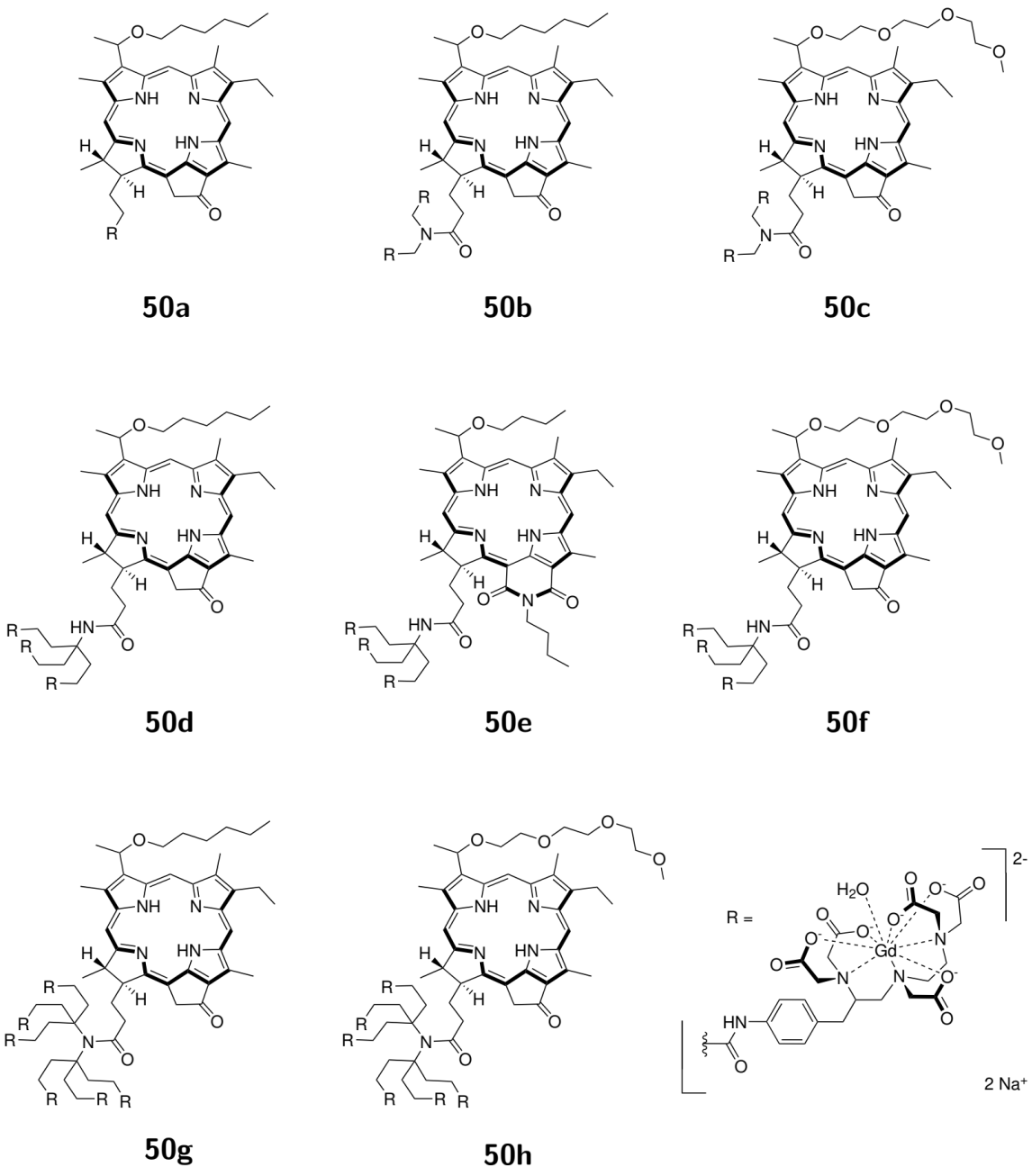

Figure 21. Ga-DTPA-modified chlorophyll A systems **50a**–**h** for a combined approach of MRI and PDT. [102–104]

as for Gd-DTPA and Gd-DOTA), which significantly reduces the T_1 relaxation time. On the other hand, the reduced stability of Gd-DTTA could lead to a higher risk for nephrogenic systemic fibrosis (NFS), an illness which is induced by gadolinium intoxication.[88,90,91,107] Since the

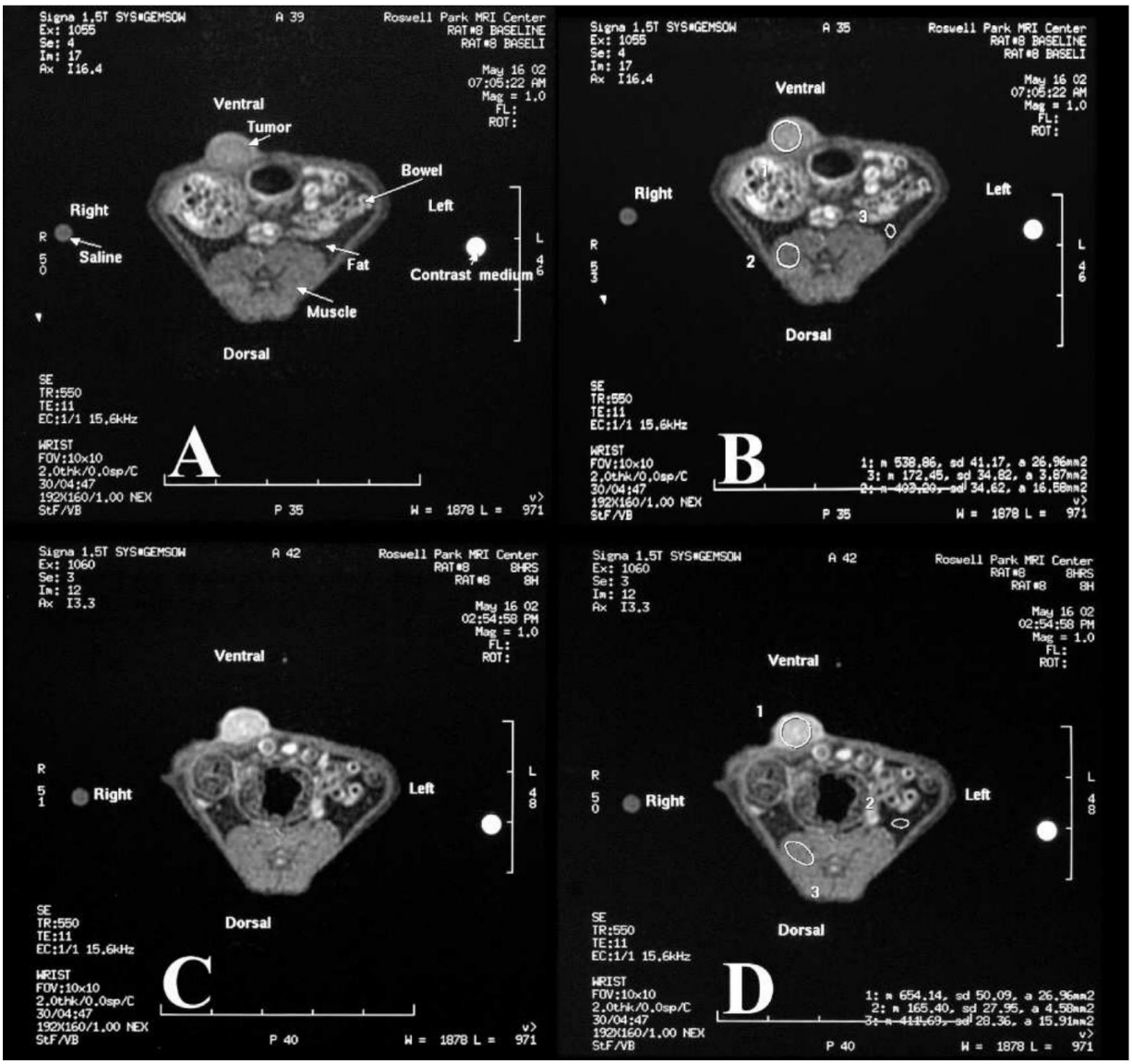

Figure 22. A: MRI of mice with a transplanted tumor ($1\,cm^3$) growing out of the abdominal wall (ventral); B: Baseline measurement of tumor (538), muscle (403), fat (172) and saline (385) and **50c** (1684) as control; C: 8 h after intravenous injection of **50c** ($10.0\,\mu mol\,kg^{-1}$) the tumor is visually enhanced; D: Baseline measurement of tumor (654), muscle (403), fat (165), saline, (359) and **50c** (1746). Reproduced with permission.[102] Copyright 2005, American Chemical Society.

probability for NFS is strongly related to the stability of a Gd(III) compound, less stable chelators like H_4DTTA could increase the probability for NFS-related medicinal complications.[107]

Nevertheless, it has to be considered that the increased r_1-relaxivity would allow for lower therapeutic doses, which could compensate the higher lability and thus result in a similar risk for NFS. The first example of such a compound (Figure 23: **51**) was published by Lou *et al.*[105] Interestingly, **51** showed a strong interaction with HSA (human serum albumin) which led to an additional reduction of the T_1 relaxation time. The cellular accumulation of **51** in H1299 (human lung cancer cell line) was strongly optimized by interaction with HSA. Since many cancer cell types have a larger tendency for HSA uptake than healthy cells, a tumor-specific accumulation of **51** could be probable and would increase the local concentration of **51** up to a higher level compared to healthy cells.[105,108] Also a raise of the r_1-relaxivity from 14.1 to 29.2mm^{-1}s^{-1} was possible by the addition of 0.6mm HSA (Table 10). Consequently, this would lead to a higher phototoxic activity and r_1-relaxivity in the malignant tissue.[105] *Via* several photochemical quenching experiments, the production of $^1O_2$ (Table 9) was confirmed.[105] A very similar compound (Figure 23: **52**) was published a few years later.[106] Interestingly, the r_1-relaxivity of **52** (Table 10: 48.6mm^{-1}s^{-1}) was significantly higher than that of **51**, even taking into account the

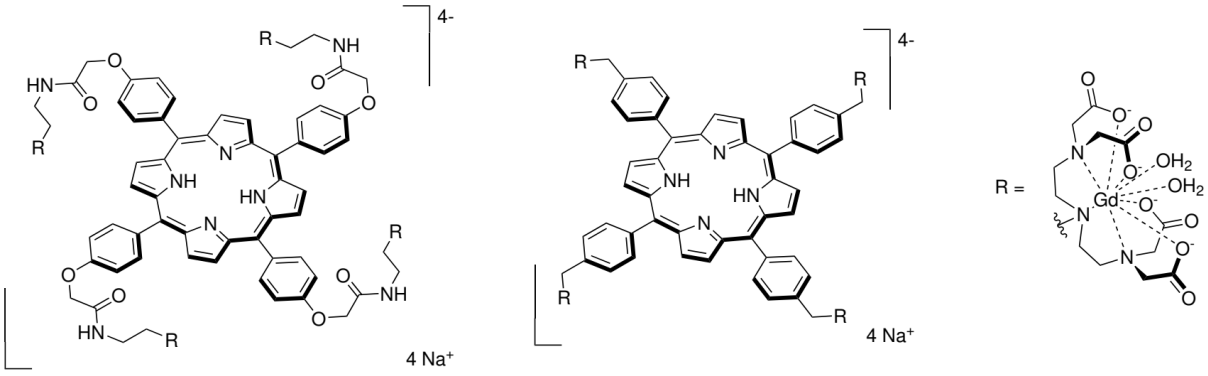

51 **52**

Figure 23. Porphyrin-based Gd(III)-DTTA complexes **51** and **52** for potential application in PDT-MRI theranostics.[105,106]

Table 9. Overview of the photophysical and biological evaluation of **50a–h**[102–104], **51**[105], **52**[106], **53a–c**[110],**54**[111], and **55**[112].

	Φ_F	Φ_Δ ([nm])	$t_{1/2}$ [ns (nm)]	IC_{50} [μM]	LD_{50} [J cm^{-2}(μM)]	λ_{max}^{Abs} [nm]
50a[102]	–	–	–	–	–	660
50b[102]	–	–	–	–	–	660
50c[102]	–	–	–	–	–	660
50d[103,104]	–	–	–	obs.[11]	$\approx$ 2.5(4.0)[11]	660
50e[103,104]	–	–	–	obs.[11]	$\approx$ 1.5(4.0)[11]	660
50f[103,104]	–	–	–	obs.[11]	–	660
50g[103,104]	–	–	–	obs.[11]	$\approx$ 2.5(4.0)[11]	660
50h[103,104]	–	–	–	obs.[11]	–	660
51[105]	0.043/75[1,8]	obs. (650)[2,7]	8.54 (375)[3]	–	–	650[1]
52[106]	0.14[1,8]	0.45 (516)[1,7]	8.50 (373)[1]	$\approx$ 50[12]	32/21 (2.5/6.0)[12]	650[1]
53a[110]	–	–	–	$\approx$ 50[13]	obs.[13]	765[4]
53b[110]	–	–	–	$>$ 50[13]	–	783[1]
53c[110]	–	–	–	$>$ 50[13]	–	790[1]
54[111]	0.15 [4,9]	0.10 (380)[1,5,6]	–	$>$ 50[14]	–	650[1]
55[112]	0.14[4,8]	0.68 (516)[1,5,10]	0.84 (465/560)[1]	$\approx$ 10[12]	9.0 (1.0)[12]	670[1]
56[113]	0.019/032[1,8]	0.21/29[1,8]	0.99/82 (465)[1]	$\approx$ 10[12]	(40.0)[12]	740[1]

[1] In H_2O.
[2] In D_2O.
[3] In HEPES.
[4] In DMSO.
[5] With DPBF (1,3-diphenylisobenzofuran) as trap molecule.
[6] With ADMA (anthracene-9,10-bismethylmalonate) as trap molecule.
[7] With ADPA (anthracene-9,10-dipropionic acid) as trap molecule.
[8] With TPP (tetraphenylporphyrin) as reference ($\Phi_\Delta = 0.11$ in toluene).
[9] With Zn(II) phthalocyanine (ZnPc) as reference ($\Phi_\Delta = 0.18$ in DMSO).
[10] With $TPPS_4$ (5,10,15,20-tetrakis(4-sulfonatophenyl)porphyrin) as reference ($\Phi_\Delta = 0.51$ in H_2O).
[11] In Colon26 & RIF-1.
[12] In HeLA.
[13] In WI-38 VA13 & A549.
[14] In MCF-7.

differences in magnetic field strengths during NMR experiments. This leads to the assumption that the effective number of coordinated water molecules in **51** is significantly smaller than the expected two because of competitive coordination of the nitrogen and oxygen atoms from the ester bonds. Cellular uptake experiments in HeLa cancer cells with CLSM showed a slow but strong accumulation of **52** in lysosomes. The $^1O_2$ production of **52** was quantified to be 45% (Table 10).[106] Their photophysical behavior is comparable with that of porphyrin-based PDT PSs, and combined with their simpler synthetic pathways it makes them interesting challengers for PDT-MRI-combined approaches. A large collection of porphyrin-based Gd-complexes as further potential fluorescent MRI contrast agents which was published by Calvete *et al.* may have potential applications in PDT. However, they will

not be discussed here since they have never been tested specifically for their PDT activity.[109]

Table 10. Overview of the relaxivity data of **50a–h**[102–104], **51**[105], **52**[106], **53a–c**[110],**54**[111] and **55**[112].

	r_1 [$mM^{-1}s^{-1}$]	r_2 [$mM^{-1}s^{-1}$]	n_{Gd}	n_{H2O}
50a[102]	–	–	1	1
50b[102]	–	–	2	1
50c[102]	18.7[1,4,11]	58.6[1,4,11]	2	1
50d[102–104]	13.5[1,4,11]	81.3[1,4,11]	3	1
50e[102–104]	11.1[1,4,11]	85.3[1,4,11]	3	1
50f[102–104]	11.6[1,4,11]	40.1[1,4,11]	3	1
50g[102–104]	24.7[1,4,11]	66.5[1,4,11]	6	1
50h[102–104]	25.1[1,4,11]	69.2[1,4,11]	6	1
51[105]	14.1/29.2[2,3,4,8]	–	4	2
52[106]	48.6[2,4,6]	–	4	2
53a[110]	4.20[2,5,9]	–	1	1
53b[110]	42.0[2,5,9]	–	4	1
53c[110]	102.4[2,5,9]	–	8	1
54[111]	1.4[2,5,10]	–	1	1
55[112]	19.9/23.9[2,3,4,7]	–	1	1
56[113]	14.4/29.7[2,3,4,7]	–	2	1
Omniscan[111]	3.2[2,5,10]	–	1	1
Magnevist[89,103,110]	4.3[1,4,11]	5.1[1,4,11]	1	1

[1] In HEPES ($pH = 7.2$).
[2] In H_2O.
[3] In H_2O + BSA.
[4] At 25 °C.
[5] At 37 °C.
[6] At 20 MHz ≈ 0.47 T.
[7] At 40 MHz ≈ 1.00 T.
[8] At 55 MHz ≈ 1.29 T.
[9] At 60 MHz ≈ 1.41 T.
[10] At 128 MHz ≈ 3.01 T.
[11] At 200 MHz ≈ 4.71 T.

Besides porphyrins, phthalocyanines are also PSs of interest. A photophysical behavior, comparable with this of porphyrins combined with their simpler syntheses makes them interesting challengers to the well-established porphyrins. The aluminiumphthalocyanine based *Photosens*® (Figure 2: **2**) which has already reached therapeutical acceptance in Russia demonstrates that metal-containing derivatives bear several advantages over metal-free phthalocyanines.[4,6,7] A series of zinc-containing phthalocyanines (ZnPc, Figure 24: **53a–c**) was published by Song *et al.* in 2010.[110] Their absorption which is located in the near-IR range up to 790nm (Table 9) is undoubtly outstanding. Complexes **53a–c** differ concerning

the number of copper-catalyzed clickchemistry-attached Gd-DOTA complexes (Table 10: **53a** = ZnPc(Gd–DOTA), **53b** = ZnPc(Gd–DOTA)$_4$ and **53c** = ZnPc(Gd–DOTA)$_8$). By increasing the amount of GdDOTA species, the r_1-relaxivity climbs from 4.2 (Table 10) up to 102.4mm^{-1}s^{-1}. By comparing the relative r_1-relaxivity proportion of each gadolinium center, the ionic r_1-relaxivity for **53c** is four times higher than for **53a**, which is a beautiful example of the PRE effect. Unfortunately, only **53a** showed significant phototoxicity, which was confirmed by cellular uptake experiments in WI-38 VA13 (non-tumorigenic, human embryonic fibroblast-like cells). Interestingly, the cellular uptake of **53a** in VA13 was ten times larger than for free Gd-DOTA.[110] Although the PRE effect has nowadays lost its importance due to the availability of strong-field MRI devices, compounds **53a–c** may still have potential for MRI-fluorescence diagnostics. A similar approach was published four years later by Aydin Tekdas et

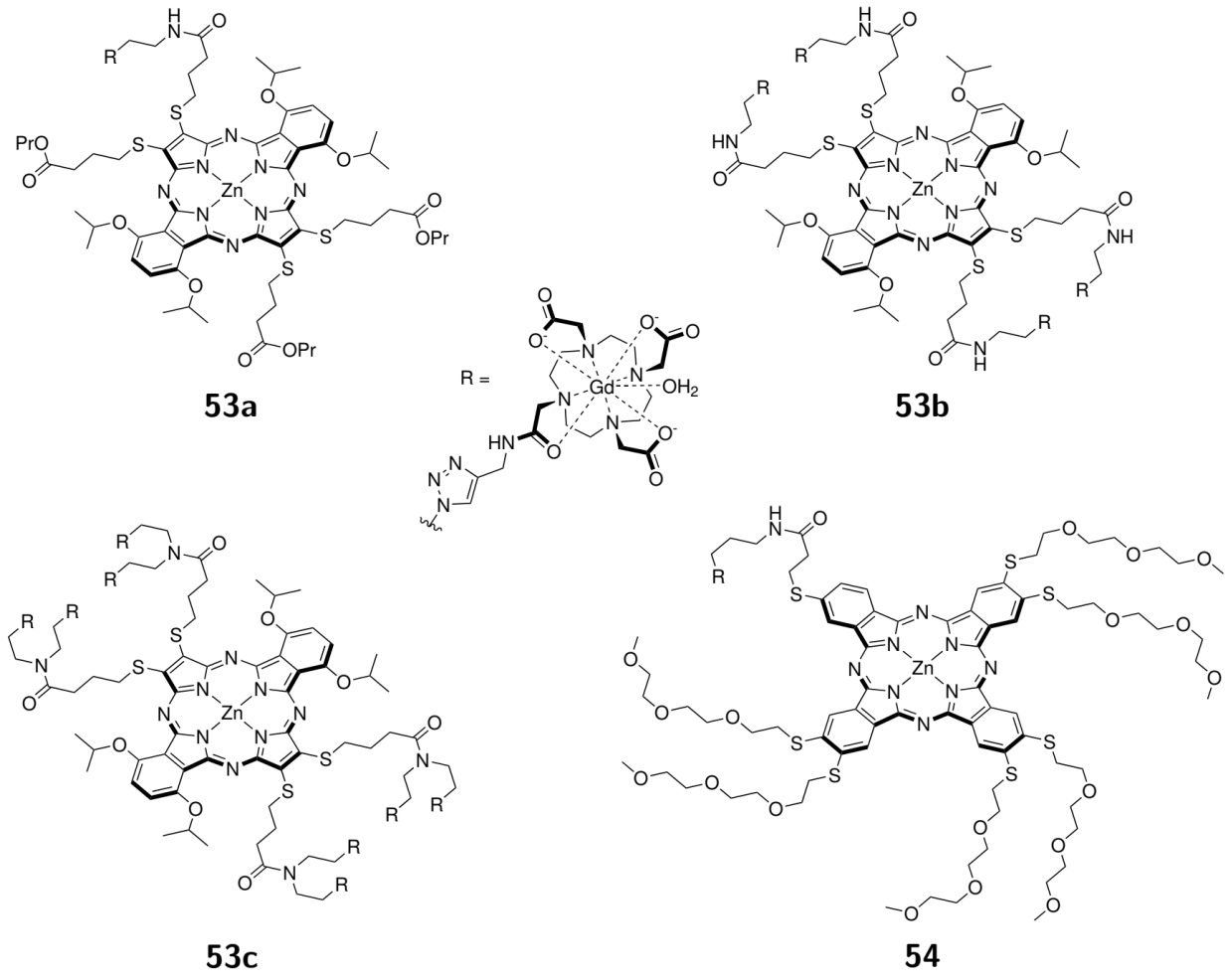

Figure 24. Neutral zinc-phtalocyanine-based bifunctional PSs **53a**–**c** and **54** for theranostic approaches. [110,111]

al.[111] The ZnPc complex **54** was designed with six polyethylene glycol (PEG) chains to achieve good ambiphilicity. It was shown that **54** had a similar $^1O_2$ quantum yield (Table 9: Φ_Δ = 0.67 in DMSO) in comparison to the PEG-modified ZnPc (ZnPc–PEG_8 Φ_Δ = 0.72) complexes.[111] On the other hand, the r_1-relaxivity of **54** (Table 10: 1.43$mm^{-1}s^{-1}$) was significantly lower than for Gd-DOTA (3.23$mm^{-1}s^{-1}$). A possible explanation is that the flexible side chain with donating atoms like the triazole, the amide or the (thio)ether could hinder the access or even compete with water

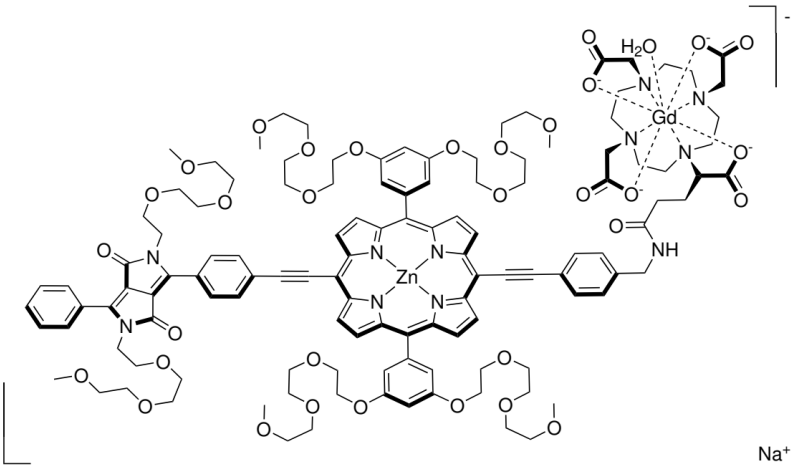

55

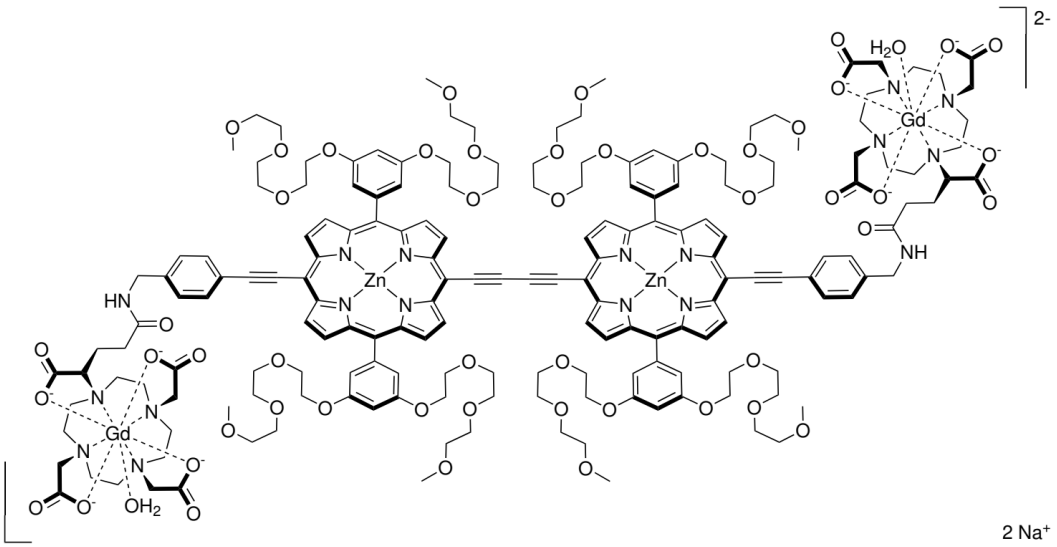

56

Figure 25. Zinc-porphyrine-based bifunctional PSs **55** and **56** by Schmitt et al. [112,113]

molecules on the gadolinium center. This would cancel out the gained r_1-relaxivity to the larger molecular size of **54**.[111] On the other hand, the *in vitro* compatibility assessments in MCF-7 (human breast cancer) cells revealed promising results with an absence of dark toxicity below a concentration of 20μm (IC_{50} >50μm).[111]

Complexes made of a combination of porphyrins, PEG chains and zinc (Figure 25: **55** and **56**) were published by Schmitt *et al.*[112,113] Interestingly, besides the one-photon absorption up

to 750nm, **55** also showed a two-photon cross-section (σ_2) of ≈ 1000GM between 910 and 940 nm.[112] Similar to **51**, compound **55** exhibited an elongation of the r_1-relaxivity from 19.9 (Table 10: 40MHz, 25°C) to 23.9$mm^{-1}s^{-1}$ upon the addition of BSA.[112] In general, the r_1-relaxivity of 19.9$mm^{-1}s^{-1}$ is relatively high for a complex with a molecular weight of 2.4kDa. The cellular uptake in HeLa cells was significantly higher for the gadolinium-free synthetic precursor of **55** in comparison to the final complex. While many of these porphyrin or phthalocyanine compounds show a strong accumulation tendency in pure water with a negative impact on photophysical and biological behavior, the aggregation of **55** was unavoidable without small concentrations of DMSO.[112] Similar to **55**, complex **56** also showed a one-photon absorption up to 750nm together with a two-photon cross-section (σ_2) of ≈1000GM between 910 and 940nm. In this compound, good photophysical and r_1-relaxivity abilities are combined with optimized solubility behaviour. Although the r_1-relaxivity in **56** (Table 10: 40MHz, 25°C) is slightly lower than for **55**, it is still four to five times higher than for commercially available MRI agents like Gd-DTPA or Gd-DOTA.[113] Cellular uptake in HeLa cells was already suitable at concentrations of 1μm with an incubation time of 24 hours. Especially remarkable is the extraordinarily high twophoton cross-section of 9400GM at 920nm (1GM = 10–50cm^4 s×$molecule^{-1}$) of **55**, which could enable a tissue penetration depth of almost 4 mm.[113] As it has been underlined in the previous examples, the combination of PDT PSs with gadolinium-containing MRI sensitive complexes could significantly increase the benefits of both systems. The theranostic abilities of MRI-PDT agents could allow for much more precise treatments of patients with less and more predictable side effects.

Conclusion

Metal complexes are currently being highly investigated as alternative PDT PSs with great success as demonstrated with TOOKAD soluble and TLD1433 discussed in this review. Recently, a sub-class of compounds, namely polymetallic complexes are gaining momentum. The considerable amount of interesting examples of polynuclear metal complexes described in this review indeed demonstrates the high potential of these compounds for future applications in PDT. We strongly believe that such complexes hold great potential, especially for personalized medicine in cancer therapy, where promising results have recently been obtained.

Author Information

Biographies

After his apprenticeship as a multimedia electronics technician, **Patrick S. Felder** studied at the University of Zurich (Switzerland), where he obtained a BSc (2015) and MSc in Chemistry (2017). In the same year, he moved to Paris (France) to start a Ph.D. thesis in the group of Gilles Gasser at Chimie ParisTech, Paris Sciences & Lettres (PSL) University. His project is related to the DFT-based development of monoand poly-metallic complexes in view of medicinal applications.

Sarah Keller obtained her Bachelor's and Master's in Chemistry at the AlbertLudwigs-University in Freiburg, Germany. In 2017, she completed her Ph.D. at the University of Basel, Switzerland, in the group of Professor Housecroft and Professor Constable working on luminescent copper(I) complexes. In 2018, she was awarded a Feoder Lynen Post-doctoral Fellowship from the Alexander von Humboldt Foundation and an Early Postoc. Mobility Fellowship from the Swiss National Science Foundation to carry out her postdoctoral research in the Gasser group at Chimie ParisTech PSL University, she is currently working on the preparation of organometallic antiparasitic drug candidates.

Gilles Gasser was born, raised, and educated in Switzerland. Gilles started his independent research career at the University of Zurich, first as Swiss National Science Foundation (SNSF) Ambizione fellow (2010) and then as a nontenure-track SNSF Assistant Professor (2011). In 2016, Gilles moved to Chimie ParisTech, Paris Sciences & Lettres (PSL) University, to take a permanent position thanks, among others, to an ERC Consolidator Grant and a PSL Chair of Excellence Program Grant. Gilles research interests lie in the use of metal complexes in medicine and chemical biology.

ORCID

Patrick S. Felder: 0000-0003-2325-9026

Sarah Keller: 0000-0003-2667-9157

Gilles Gasser: 0000-0002-4244-5097

Notes

The authors declare no competing financial interest.

Acknowledgment

This work was financially supported by an ERC Consolidator Grant PhotoMedMet to G.G. (GA 681679) and has received support under the program “Investissements d’Avenir” launched by the French Government and implemented by the ANR with the reference ANR-10-IDEX-0001-02 PSL (G.G.). It was further supported by a Feodor Lynen Research Fellowship from the Alexander von Humboldt Foundation (S.K.) as well as an Early Postdoc. Mobility Fellowship from the Swiss National Science Foundation (S.K., Grant P2 BSP2_181760).

Table of content

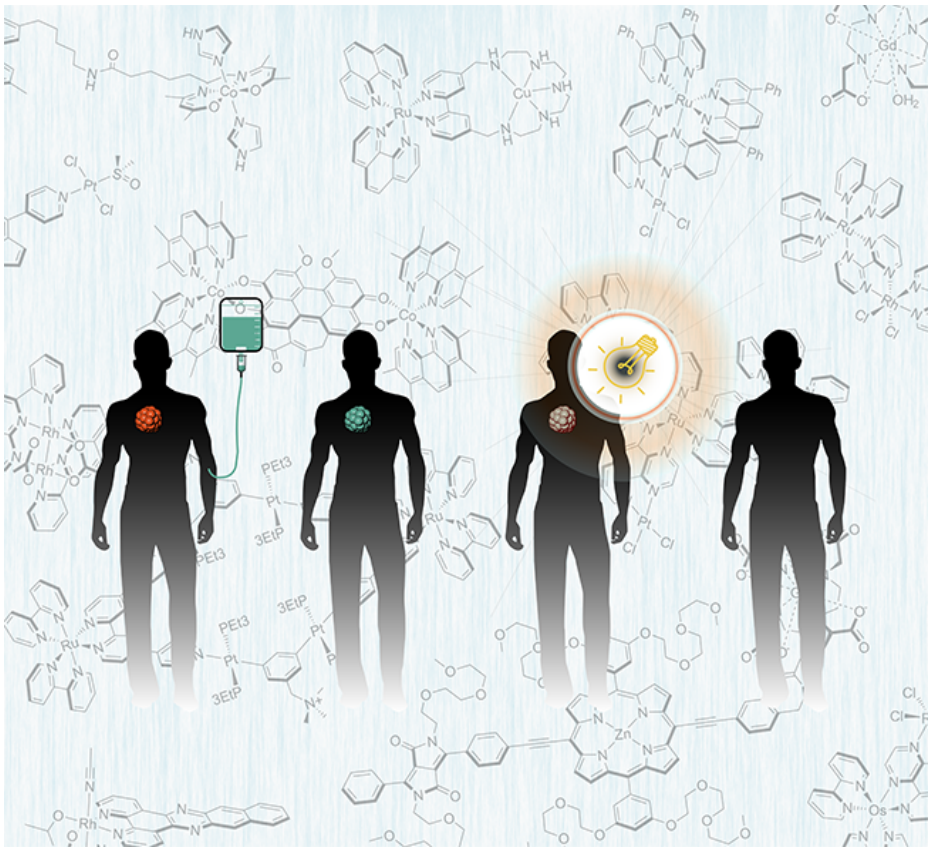

References

[1] F. Heinemann, J. Karges, G. Gasser, *Acc Chem Res* **2017**, *50*, 2727-2736.

[2] J. Kou, D. Dou, L. Yang, *Oncotarget* **2017**, *8*, 81591-81603.

[3] S. Monro, K. L. Colon, H. Yin, J. Roque, 3rd, P. Konda, S. Gujar, R. P. Thummel, L. Lilge, C. G. Cameron, S. A. McFarland, *Chem Rev* **2019**, *119*, 797-828.

[4] E. A. Lukyanets, *Journal of Porphyrins and Phthalocyanines* **2012**, *03*, 424-432.

[5] E. F. Stranadko, *Biomedical Photonics* **2015**, *4*, 3-10.

[6] A. A. Brilkina, L. V. Dubasova, E. A. Sergeeva, A. J. Pospelov, N. Y. Shilyagina, N. M. Shakhova, I. V. Balalaeva, *J Photochem Photobiol B* **2019**, *191*, 128-134.

[7] X. Li, B.-D. Zheng, X.-H. Peng, S.-Z. Li, J.-W. Ying, Y. Zhao, J.-D. Huang, J. Yoon, *Coordination Chemistry Reviews* **2019**, *379*, 147-160.

[8] https://www.ema.europa.eu/en/medicines/human/EPAR/tookad, Accessed on: 19.05.2019

[9] A. R. Azzouzi, S. Vincendeau, E. Barret, A. Cicco, F. Kleinclauss, H. G. van der Poel, C. G. Stief, J. Rassweiler, G. Salomon, E. Solsona, A. Alcaraz, T. T. Tammela, D. J. Rosario, F. Gomez-Veiga, G. Ahlgren, F. Benzaghou, B. Gaillac, B. Amzal, F. M. Debruyne, G. Fromont, C. Gratzke, M. Emberton, P. C. M. S. Group, *Lancet Oncol* **2017**, *18*, 181-191.

[10] https://clinicaltrials.gov/ct2/show/NCT03849365, Accessed on: 19.05.2019

[11] A. E. O'Connor, W. M. Gallagher, A. T. Byrne, *Photochem Photobiol* **2009**, *85*, 1053-1074.

[12] https://clinicaltrials.gov/ct2/show/NCT03053635, Accessed on: 19.05.2019

[13] J. Zhang, C. Jiang, J. P. Figueiro Longo, R. B. Azevedo, H. Zhang, L. A. Muehlmann, *Acta Pharm Sin B* **2018**, *8*, 137-146.

[14] C. A. Lipinski, F. Lombardo, B. W. Dominy, P. J. Feeney, *Advanced Drug Delivery Reviews* **2001**, *46*, 3-26.

[15] S. Ben-Dror, I. Bronshtein, A. Wiehe, B. Roder, M. O. Senge, B. Ehrenberg, *Photochem Photobiol* **2006**, *82*, 695-701.

[16] S. Diwu, C. Zhang, J. W. Lown, *Journal of Photochemistry and Photobiology A: Chemistry* **1992**, *66*, 99-112.

[17] J.-Y. An, F. Tian, Y.-Z. Hu, L.-J. Jiang, *Chinese Journal of Chemistry* **2010**, *11*, 532-539.

[18] D. Wang, J. Zhou, R. Shi, H. Wu, R. Chen, B. Duan, G. Xia, P. Xu, H. Wang, S. Zhou, C. Wang, H. Wang, Z. Guo, Q. Chen, *Theranostics* **2017**, *7*, 4605-4617.

[19] J. Ma, J. Zhao, L. Jiang, *New Journal of Chemistry* **2001**, *25*, 847-852.

[20] H. Maeda, J. Wu, T. Sawa, Y. Matsumura, K. Hori, *J Control Release* **2000**, *65*, 271-284.

[21] Z. Zeng, J. Zhou, Y. Zhang, R. Qiao, S. Xia, J. Chen, X. Wang, B. Zhang, *J Phys Chem B* **2007**, *111*, 2688-2696.

[22] L. Zhou, X. Ge, J. Liu, J. Zhou, S. Wei, F. Li, J. Shen, *Bioorg Med Chem Lett* **2013**, *23*, 5317-5324.

[23] J. Zhou, J. Liu, Y. Feng, S. Wei, X. Gu, X. Wang, B. Zhang, *Bioorg Med Chem Lett* **2005**, *15*, 3067-3070.

[24] Y. Sun, Y. J. Hou, Q. X. Zhou, W. H. Lei, J. R. Chen, X. S. Wang, B. W. Zhang, *Inorg Chem* **2010**, *49*, 10108-10116.

[25] Y. Sun, Y. J. Hou, Q. X. Zhou, J. R. Chen, B. W. Zhang, X. S. Wang, *J Inorg Biochem* **2011**, *105*, 978-984.

[26] K. Ogawa, Y. Kobuke, *Anticancer Agents Med Chem* **2008**, *8*, 269-279.

[27] K. Plaetzer, B. Krammer, J. Berlanda, F. Berr, T. Kiesslich, *Lasers Med Sci* **2009**, *24*, 259-268.

[28] M. Hayyan, M. A. Hashim, I. M. AlNashef, *Chem Rev* **2016**, *116*, 3029-3085.

[29] R. P. Wayne, in *Advances in Photochemistry*, **2007**, pp. 311-371.

[30] C. M. Marian, *Wiley Interdisciplinary Reviews: Computational Molecular Science* **2012**, *2*, 187-203.

[31] C. L. Yang, X. W. Zhang, H. You, L. Y. Zhu, L. Q. Chen, L. N. Zhu, Y. T. Tao, D. G. Ma, Z. G. Shuai, J. G. Qin, *Advanced Functional Materials* **2007**, *17*, 651-661.

[32] M. Ucuncu, E. Karakus, E. Kurulgan Demirci, M. Sayar, S. Dartar, M. Emrullahoglu, *Org Lett* **2017**, *19*, 2522-2525.

[33] R. Padilla, R. R. Ruminski, V. A. Meredith McGinley, P. B. Williams, *Polyhedron* **2012**, *33*, 158-165.

[34] R. R. Ruminski, J. A. Canaria, R. Padilla, *Inorganica Chimica Acta* **2013**, *401*, 95-100.

[35] S. Swavey, K. J. Brewer, *Inorg Chem* **2002**, *41*, 6196-6198.

[36] A. A. Holder, S. Swavey, K. J. Brewer, *Inorg Chem* **2004**, *43*, 303-308.

[37] A. A. Holder, D. F. Zigler, M. T. Tarrago-Trani, B. Storrie, K. J. Brewer, *Inorg Chem* **2007**, *46*, 4760-4762.

[38] J. Wang, S. L. Higgins, B. S. Winkel, K. J. Brewer, *Chem Commun (Camb)* **2011**, *47*, 9786-9788.

[39] J. Wang, D. F. Zigler, N. Hurst, H. Othee, B. S. Winkel, K. J. Brewer, *J Inorg Biochem* **2012**, *116*, 135-139.

[40] J. Wang, J. Newman, Jr., S. L. Higgins, K. M. Brewer, B. S. Winkel, K. J. Brewer, *Angew Chem Int Ed Engl* **2013**, *52*, 1262-1265.

[41] P. M. Bradley, B. E. Bursten, C. Turro, *Inorg Chem* **2001**, *40*, 1376-1379.

[42] K. Sorasaenee, P. K. Fu, A. M. Angeles-Boza, K. R. Dunbar, C. Turro, *Inorg Chem* **2003**, *42*, 1267-1271.

[43] P. M. Bradley, A. M. Angeles-Boza, K. R. Dunbar, C. Turro, *Inorg Chem* **2004**, *43*, 2450-2452.

[44] H. T. Chifotides, P. K. Fu, K. R. Dunbar, C. Turro, *Inorg Chem* **2004**, *43*, 1175-1183.

[45] A. M. Angeles-Boza, P. M. Bradley, P. K. Fu, M. Shatruk, M. G. Hilfiger, K. R. Dunbar, C. Turro, *Inorg Chem* **2005**, *44*, 7262-7264.

[46] A. M. Angeles-Boza, H. T. Chifotides, J. D. Aguirre, A. Chouai, P. K. Fu, K. R. Dunbar, C. Turro, *J Med Chem* **2006**, *49*, 6841-6847.

[47] J. D. Aguirre, D. A. Lutterman, A. M. Angeles-Boza, K. R. Dunbar, C. Turro, *Inorg Chem* **2007**, *46*, 7494-7502.

[48] J. D. Aguirre, A. M. Angeles-Boza, A. Chouai, J. P. Pellois, C. Turro, K. R. Dunbar, *J Am Chem Soc* **2009**, *131*, 11353-11360.

[49] L. E. Joyce, J. D. Aguirre, A. M. Angeles-Boza, A. Chouai, P. K. Fu, K. R. Dunbar, C. Turro, *Inorg Chem* **2010**, *49*, 5371-5376.

[50] A. Naik, R. Rubbiani, G. Gasser, B. Spingler, *Angew Chem Int Ed Engl* **2014**, *53*, 6938-6941.

[51] F. Schmitt, P. Govindaswamy, G. Suss-Fink, W. H. Ang, P. J. Dyson, L. Juillerat-Jeanneret, B. Therrien, *J Med Chem* **2008**, *51*, 1811-1816.

[52] M. Pernot, T. Bastogne, N. P. Barry, B. Therrien, G. Koellensperger, S. Hann, V. Reshetov, M. Barberi-Heyob, *J Photochem Photobiol B* **2012**, *117*, 80-89.

[53] R. Miao, M. T. Mongelli, D. F. Zigler, B. S. Winkel, K. J. Brewer, *Inorg Chem* **2006**, *45*, 10413-10415.

[54] Z. Zhou, J. Liu, T. W. Rees, H. Wang, X. Li, H. Chao, P. J. Stang, *Proc Natl Acad Sci U S A* **2018**, *115*, 5664-5669.

[55] D. Luo, K. A. Carter, D. Miranda, J. F. Lovell, *Adv Sci (Weinh)* **2017**, *4*, 1600106.

[56] E. Wong, C. M. Giandomenico, *Chem Rev* **1999**, *99*, 2451-2466.

[57] F. Lentz, A. Drescher, A. Lindauer, M. Henke, R. A. Hilger, C. G. Hartinger, M. E. Scheulen, C. Dittrich, B. K. Keppler, U. Jaehde, E. Central European Society for Anticancer Drug Research, *Anticancer Drugs* **2009**, *20*, 97-103.

[58] C. G. Hartinger, S. Zorbas-Seifried, M. A. Jakupec, B. Kynast, H. Zorbas, B. K. Keppler, *J Inorg Biochem* **2006**, *100*, 891-904.

[59] R. Trondl, P. Heffeter, C. R. Kowol, M. A. Jakupec, W. Berger, B. K. Keppler, *Chem. Sci.* **2014**, *5*, 2925-2932.

[60] A. Notaro, G. Gasser, *Chemical Society Reviews* **2017**, *46*, 7317--7337.

[61] S. L. Higgins, T. A. White, B. S. Winkel, K. J. Brewer, *Inorg Chem* **2011**, *50*, 463-470.

[62] S. L. Higgins, A. J. Tucker, B. S. Winkel, K. J. Brewer, *Chem Commun (Camb)* **2012**, *48*, 67-69.

[63] J. Zhu, J. A. Rodriguez-Corrales, R. Prussin, Z. Zhao, A. Dominijanni, S. L. Hopkins, B. S. Winkel, J. L. Robertson, K. J. Brewer, *Chem Commun (Camb)* **2016**, *53*, 145-148.

[64] J. D. Knoll, C. Turro, *Coord Chem Rev* **2015**, *282-283*, 110-126.

[65] R. Padilla, W. A. Maza, A. J. Dominijanni, B. S. J. Winkel, A. J. Morris, K. J. Brewer, *Journal of Photochemistry and Photobiology A: Chemistry* **2016**, *322-323*, 67-75.

[66] L. Zeng, P. Gupta, Y. Chen, E. Wang, L. Ji, H. Chao, Z.-S. Chen, J. Mai, H. Zhang, Z. Li, M. Guevara, Z. W. Mao, H. Shen, G. Superti-Furga, B. K. Keppler, C. G. Hartinger, *Chem. Soc. Rev.* **2017**, *46*, 5771--5804.

[67] M. Jakubaszek, B. Goud, S. Ferrari, G. Gasser, *Chem Commun (Camb)* **2018**, *54*, 13040-13059.

[68] J. K. Barton, L. A. Basile, A. Danishefsky, A. Alexandrescu, *Proc Natl Acad Sci U S A* **1984**, *81*, 1961-1965.

[69] C. V. Kumar, J. K. Barton, N. J. Turro, *Journal of the American Chemical Society* **1985**, *107*, 5518-5523.

[70] A. Sitlani, E. C. Long, A. M. Pyle, J. K. Barton, *Journal of the American Chemical Society* **1992**, *114*, 2303-2312.

[71] K. B. Brewer, VA, US), Swavey, Shawn (Kettering, OH, US), Supramolecular complexes as photoactivated DNA cleavage agents, **2003**, Patent Nr. 20030180767, http://www.freepatentsonline.com/y2003/0180767.html

[72] K. B. Brewer, VA, US), Swavey, Shawn (Kettering, OH, US), Supramolecular complexes as photoactivated DNA cleavage agents, **2005**, Patent Nr. 20050272713, http://www.freepatentsonline.com/y2005/0272713.html

[73] K. B. Brewer, VA, US), Swavey, Shawn (Springboro, OH, US), Supramolecular complexes as photoactivated DNA cleavage agents, **2010**, Patent Nr. 20100047910, http://www.freepatentsonline.com/y2010/0047910.html

[74] S. Mardanya, S. Karmakar, D. Mondal, S. Baitalik, *Inorg Chem* **2016**, *55*, 3475-3489.

[75] S. Swavey, M. Wang, *Inorganic Chemistry Communications* **2015**, *61*, 228-230.

[76] L. Conti, A. Bencini, C. Ferrante, C. Gellini, P. Paoli, M. Parri, G. Pietraperzia, B. Valtancoli, C. Giorgi, *Chemistry* **2019**, *25*, 10606-10615.

[77] R. J. Holbrook, D. J. Weinberg, M. D. Peterson, E. A. Weiss, T. J. Meade, *J Am Chem Soc* **2015**, *137*, 3379-3385.

[78] J. A. Schwartz, E. K. Lium, S. J. Silverstein, *J Virol* **2001**, *75*, 4117-4128.

[79] M. C. Heffern, N. Yamamoto, R. J. Holbrook, A. L. Eckermann, T. J. Meade, *Curr Opin Chem Biol* **2013**, *17*, 189-196.

[80] W. R. Browne, A. A. Holder, M. A. Lawrence, J. L. Bullock Jr, L. Lilge, *Ruthenium Complexes*, **2018**.

[81] C. M. Partigianoni, C. Turró, C. Hsu, I. J. Chang, D. G. Nocera, in *Photosensitive Metal—Organic Systems*, **1993**, pp. 147-163.

[82] H. T. Chifotides, K. R. Dunbar, *Acc Chem Res* **2005**, *38*, 146-156.

[83] H. T. Chifotides, K. M. Koshlap, L. M. Perez, K. R. Dunbar, *J Am Chem Soc* **2003**, *125*, 10703-10713.

[84] P. K. Fu, P. M. Bradley, C. Turro, *Inorg Chem* **2001**, *40*, 2476-2477.

[85] J. B. Hudson, J. Zhou, J. Chen, L. Harris, L. Yip, G. H. Towers, *Photochem Photobiol* **1994**, *60*, 253-255.

[86] Z. Diwu, *Photochem Photobiol* **1995**, *61*, 529-539.

[87] Y.-Z. Hu, J.-Y. An, L.-J. Jiang, *Journal of Photochemistry and Photobiology B: Biology* **1994**, *22*, 219-227.

[88] Y. Jeong, H. S. Hwang, K. Na, *Biomater Res* **2018**, *22*, 20.

[89] R. B. Lauffer, T. J. Brady, *Magn Reson Imaging* **1985**, *3*, 11-16.

[90] E. Blumfield, D. W. Swenson, R. S. Iyer, A. L. Stanescu, *Pediatr Radiol* **2019**, *49*, 448-457.

[91] J. Wahsner, E. M. Gale, A. Rodriguez-Rodriguez, P. Caravan, *Chem Rev* **2019**, *119*, 957-1057.

[92] D. R. Burton, S. Forsen, G. Karlstrom, R. A. Dwek, *Progress in Nuclear Magnetic Resonance Spectroscopy* **1979**, *13*, 1-45.

[93] M. L. Wood, P. A. Hardy, *J Magn Reson Imaging* **1993**, *3*, 149-156.

[94] S. Aime, M. Botta, M. Fasano, E. Terreno, *Spectrochimica Acta Part A: Molecular Spectroscopy* **1993**, *49*, 1315-1322.

[95] J. B. Livramento, A. Sour, A. Borel, A. E. Merbach, E. Toth, *Chemistry* **2006**, *12*, 989-1003.

[96] V. Comblin, D. Gilsoul, M. Hermann, V. Humblet, V. Jacques, M. Mesbahi, C. Sauvage, J. F. Desreux, *Coordination Chemistry Reviews* **1999**, *185-186*, 451-470.

[97] J. Paris, C. Gameiro, V. Humblet, P. K. Mohapatra, V. Jacques, J. F. Desreux, *Inorg Chem* **2006**, *45*, 5092-5102.

[98] J. Costa, R. Ruloff, L. Burai, L. Helm, A. E. Merbach, *J Am Chem Soc* **2005**, *127*, 5147-5157.

[99] L. Moriggi, A. Aebischer, C. Cannizzo, A. Sour, A. Borel, J. C. Bunzli, L. Helm, *Dalton Trans* **2009**, 2088-2095.

[100] A. Nithyakumar, V. Alexander, *New Journal of Chemistry* **2016**, *40*, 4606-4616.

[101] T. Koullourou, L. S. Natrajan, H. Bhavsar, S. J. Pope, J. Feng, J. Narvainen, R. Shaw, E. Scales, R. Kauppinen, A. M. Kenwright, S. Faulkner, *J Am Chem Soc* **2008**, *130*, 2178-2179.

[102] G. Li, A. Slansky, M. P. Dobhal, L. N. Goswami, A. Graham, Y. Chen, P. Kanter, R. A. Alberico, J. Spernyak, J. Morgan, R. Mazurchuk, A. Oseroff, Z. Grossman, R. K. Pandey, *Bioconjug Chem* **2005**, *16*, 32-42.

[103] L. N. Goswami, W. H. White, 3rd, J. A. Spernyak, M. Ethirajan, Y. Chen, J. R. Missert, J. Morgan, R. Mazurchuk, R. K. Pandey, *Bioconjug Chem* **2010**, *21*, 816-827.

[104] J. A. Spernyak, W. H. White, 3rd, M. Ethirajan, N. J. Patel, L. Goswami, Y. Chen, S. Turowski, J. R. Missert, C. Batt, R. Mazurchuk, R. K. Pandey, *Bioconjug Chem* **2010**, *21*, 828-835.

[105] J. Luo, L. F. Chen, P. Hu, Z. N. Chen, *Inorg Chem* **2014**, *53*, 4184-4191.

[106] A. Sour, S. Jenni, A. Orti-Suarez, J. Schmitt, V. Heitz, F. Bolze, P. Loureiro de Sousa, C. Po, C. S. Bonnet, A. Pallier, E. Toth, B. Ventura, *Inorg Chem* **2016**, *55*, 4545-4554.

[107] A. K. Abu-Alfa, *Adv Chronic Kidney Dis* **2011**, *18*, 188-198.

[108] E. Frei, *Diabetol Metab Syndr* **2011**, *3*, 11.

[109] M. J. F. Calvete, S. M. A. Pinto, M. M. Pereira, C. F. G. C. Geraldes, *Coordination Chemistry Reviews* **2017**, *333*, 82-107.

[110] Y. Song, H. Zong, E. R. Trivedi, B. J. Vesper, E. A. Waters, A. G. Barrett, J. A. Radosevich, B. M. Hoffman, T. J. Meade, *Bioconjug Chem* **2010**, *21*, 2267-2275.

[111] D. Aydin Tekdas, R. Garifullin, B. Senturk, Y. Zorlu, U. Gundogdu, E. Atalar, A. B. Tekinay, A. A. Chernonosov, Y. Yerli, F. Dumoulin, M. O. Guler, V. Ahsen, A. G. Gurek, *Photochem Photobiol* **2014**, *90*, 1376-1386.

[112] J. Schmitt, V. Heitz, A. Sour, F. Bolze, P. Kessler, L. Flamigni, B. Ventura, C. S. Bonnet, E. Toth, *Chemistry* **2016**, *22*, 2775-2786.

[113] J. Schmitt, S. Jenni, A. Sour, V. Heitz, F. Bolze, A. Pallier, C. S. Bonnet, E. Toth, B. Ventura, *Bioconjug Chem* **2018**, *29*, 3726-3738.